Coupled modeling of irradiated fuel thermochemistry and gas diffusion during severe accidents

A. Germain, J. Sercombe, C. Riglet-Martial, C. Introïni, L. Noirot, Y. Pontillon, Ph H Maugis

▶ **To cite this version:**

A. Germain, J. Sercombe, C. Riglet-Martial, C. Introïni, L. Noirot, et al.. Coupled modeling of irradiated fuel thermochemistry and gas diffusion during severe accidents. Journal of Nuclear Materials, 2022, 560, pp.153429. 10.1016/j.jnucmat.2021.153429 . hal-04018893

HAL Id: hal-04018893
https://amu.hal.science/hal-04018893

Submitted on 23 Mar 2023

HAL is a multi-disciplinary open access archive for the deposit and dissemination of scientific research documents, whether they are published or not. The documents may come from teaching and research institutions in France or abroad, or from public or private research centers.

L'archive ouverte pluridisciplinaire **HAL**, est destinée au dépôt et à la diffusion de documents scientifiques de niveau recherche, publiés ou non, émanant des établissements d'enseignement et de recherche français ou étrangers, des laboratoires publics ou privés.

Coupled modeling of irradiated fuel thermochemistry and gas diffusion during severe accidents

A. Germain[a], J. Sercombe[a*], C. Riglet-Martial[a], C. Introïni[a], L. Noirot[a], Y. Pontillon[a] and Ph. Maugis[b]

[a] CEA, DES, IRESNE, DEC, 13018 Saint-Paul-Lez-Durance, France
[b] Aix-Marseille University, CNRS, IM2NP, 13397 Marseille, France

Accepted version, December 10, 2021

Abstract

In this paper, a novel approach where irradiated fuel thermochemistry and gas release are coupled is presented in details and illustrated by the simulations of some tests of the VERCORS program characterized by increasing temperatures and varying gas composition in the furnace (oxidizing or reducing conditions). At each step of the tests, the oxidation/reduction of the nuclear fuel and the fission product chemical speciation are precisely assessed thanks to a thermochemical equilibrium calculation relying on the OpenCalphad thermochemical solver and on a built-in thermochemical database derived from the SGTE database and completed by a solid solution model for the U-O-fission product system. Fission products releases are estimated from the chemically reactive gases that form in the fuel (according to the thermochemical calculation) and from a gas diffusion model based on the equivalent sphere model. The gas diffusion model takes into account not only the noble gases available in the fuel prior to the test but also the chemically reactive gases that form during the test.

It is shown that the proposed coupled approach provides a consistent estimation of fission product release (I, Te, Cs, Mo, Ba) during the VERCORS tests in spite of the simple gas diffusion mechanism considered in the simulations (no distinction between the fission products). The proposed coupled approach is used to test some thermochemical hypotheses to improve the calculated release of some fission products (Ba, Mo).

Introduction

Estimation of the Fission Product (FP) release from a nuclear reactor in case of a severe accident is of major importance for decision making during a potential crisis, as shown by past severe accidents and especially during Fukushima. To better assess the thermodynamic conditions of importance with respect to the release of FPs, many experimental programs have been launched worldwide [1]. Integral tests (rod assembly scale) such as PHEBUS-FP [2] or separate-effect tests (fuel rod scale) such as HEVA [3], VERCORS [4][5][6][7] or more recently VERDON [8][9][10] at CEA, have provided meaningful results on the impact of temperature, oxygen potential, fuel burnup, fuel fragmentation on FP release.

These programs led to the classification of FPs in four main categories: volatile, semi-volatile, low volatile and non-volatile [7]. The volatile FPs include Xe, Kr, I, Cs, Te, Sb, Cd, Rb, Ag which are almost totally released at the end of the tests and not sensitive in term of final release to the external conditions (i.e. thermochemistry), whether oxidizing or reducing. The semi-volatile FPs include Mo, Ba, Rh, Tc and Pd. The fraction released (50 to 100%) and the release kinetics depend strongly on the atmosphere in contact with the fuel and on the cladding. For example, the release of Mo is inhibited in reducing conditions while that of Ba is increased. In an oxidizing atmosphere, this trend is reversed: Mo release is favored while Ba release is inhibited. Part of the Ba was also found to react with the cladding once freed from the fuel. The low-volatile FPs include Ru, Ce, Sr, Y, Eu, Nb. Their release is generally lower than 10% of their initial inventory but it can vary as a function of atmospheric conditions or sample characteristics. Other FPs, most actinides, U and Zr, are non-volatile regardless of the experimental conditions (i.e., final release less than 1%). These results highlight the crucial importance of the chemical speciation of FPs in the fuel with regards to the release kinetics during the tests.

For this reason, codes dedicated to severe accident modeling usually include thermochemical calculations of the FP state within the fuel and of the solid-gas equilibria at the fuel surface, fuel oxidation kinetics models, clad oxidation models and FPs diffusion models. This is the case of the ASTEC code developed by IRSN (France) [11][12], the VICTORIA code developed by the NRC (USA) [13], the MELCOR code developed by the Sandia National Laboratory for the NRC (USA) [14] or the MFPR code developed by IBRAE (Russia) [15][16]. The complexity of the models in these codes depends mainly on the purpose of the codes whether they are intended to perform integrated analyses (eg., ASTEC) or to study specific aspects of severe accidents (eg., MFPR). In recent years, some fuel performance codes dealing with normal operating conditions have been upgraded to include a description of FP thermochemistry and oxygen redistribution in the fuel as, for example, PLEIADES/ALCYONE developed by the CEA [17]. Power transient simulations with temperature values at the fuel pellet center exceeding 2200 K led to interesting results showing also the importance of the chemical speciation of FPs (I, Te, Cs, Mo) on their release kinetics [18][19]. While far from the oxidizing conditions encountered

in severe accident conditions, these simulations rely on the coupling of a mechanistic fission gas release model, MARGARET [20], with thermochemical equilibrium calculations performed at each time step and radial position in the discretized fuel pellet [21]. Contrary to what is usually done in severe accident codes, the FPs are assumed to react freely with each other in the fuel. The gaseous species formed are then released at the same rate which rely on the release kinetics of the most abundant (and chemically inert) FPs, Xe and Kr. The differences in FP release are thus only related to their chemical state in the fuel. For example, a low release of Cs was obtained compared to I and Te, mostly due to the immobilization of Cs in $Cs_2MoO_{4(l,s)}$ at high temperatures [18]. Validation of this coupled model relies on radial profiles of FPs in the fuel pellet measured at the end of the power transient but does not include data on release kinetics.

In this paper, the coupled approach available in PLEIADES/ALCYONE has been extended to severe accident conditions. The VERCORS/VERDON tests provide an extensive database for FPs release kinetics validation since on-line gamma spectrometry measurements for most of the FPs are available. This work represents a first step towards a unified treatment of nominal and severe accident conditions within a single fuel performance code. The paper is organized as follows. First, the extension of the thermodynamic database used for normal operating conditions (reducing) to highly oxidizing conditions is detailed. Second, the gas diffusion model used for annealing tests is presented. Third, the coupling between irradiated fuel thermochemistry and gas diffusion is discussed and release kinetics obtained for Xe, I, Te, Cs, Mo and Ba during a selection of VERCORS tests are compared to on-line measurements. The importance of the cladding at high temperature and of the injected gas composition on Ba and Mo are then discussed.

1 Modelling of irradiated fuel thermochemistry

The modeling of irradiated fuel thermochemistry is based on the approach adopted in PLEIADES ALCYONE for normal operating conditions [18]. The VERCORS tests are performed on small fuel rodlets pre-irradiated in commercial reactors. An accurate quantification of the initial inventory of FPs in the fuel is first necessary to perform thermochemical calculations. It relies on calculations of the reactor irradiation history with the depletion code CESAR [22] that takes into account more than 200 isotopes of the main FPs. In fact, stable FP content vary quasi-linearly with burnup (up to at least 10 at%) for a given initial fuel enrichment. It is therefore common practice to use empirical linear correlations with burnup to define the initial inventory of FPs. Another common practice is the gathering of FPs in series of representative elements to reduce the size of the chemical system and thus potential convergence errors [18][23]. Each representative element includes FPs with a similar chemical behavior and is named after the most abundant one. The gathering of FPs in 14 representative elements used by Baurens et al. [18] in PLEIADES/ALCYONE is illustrated in figure 1 for the fuel section of the VERCORS 4 and 5 tests [4] taken from the same father rod (average burnup of the rodlets 38 GWd/tU).

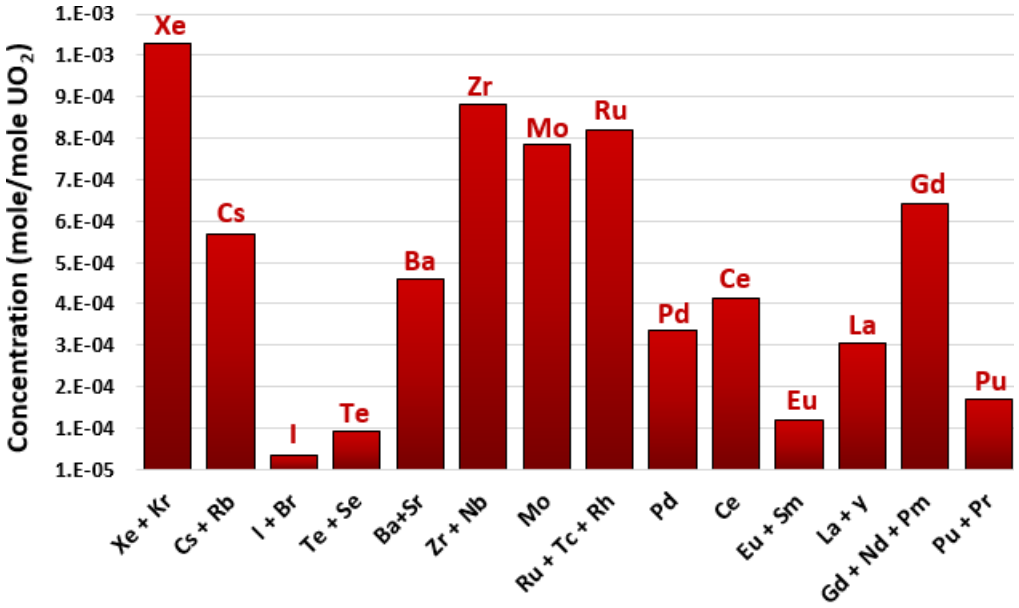

Figure 1: Initial FPs inventory calculated for the rodlets of the VERCORS (4 or 5) tests (average burnup of 38 GWd/tU).

The representative elements include noble gases (Xe + Kr), volatile FPs (Cs + Rb), (I + Br), (Te + Se), semi-volatile FPs (Ba + Sr), (Mo), low volatile FPs (Zr + Nb), (Ru + Tc + Rh), (Pd), (Ce), (Eu + Sm), (La + Y), (Gd + Nd + Pm) and actinides (Pu + Pr). In spite of their small release, rare earth are important for thermochemical equilibrium calculations since they dissolve easily in the fuel matrix.

To date, the thermochemical equilibrium calculations on the 14 element system at given temperature and pressure are performed in PLEIADES/ALCYONE with the OpenCalphad (OC) open source software [21],[24],[25]. The thermochemical database used for normal operating conditions in PLEIADES/ALCYONE is called TBASE and was originally developed to be representative of the anoxic conditions taking place within non-failed fuel rods. The thermodynamic data for all the compounds likely to form in the fuel were taken from the SGPS-SGTE pure substance database [26] of the commercial software FactSage 7.2 (FS). Cross-comparisons with OC equilibrium calculations were first used to check the validity of the initial TBASE database. Following the same protocol, the extension to severe accident conditions required the introduction of many additional compounds (hydrogen-based compounds among others). The complete list of phases and compounds included in the extended TBASE database is given in Appendix A.

In a previous paper of our group [27], thermochemical calculations results on the VERCORS 4 and VERCORS 5 tests with FS and OC have been compared to check the implementation of

the new compounds in the TBASE. The two test sequences are representative of the temperature and external conditions (H_2 and H_2O content of the injected gas phase in contact with the fuel rodlet) occurring during severe accidents. This validation exercise showed that quasi identical chemical speciation of the volatile and semi-volatile FPs (I, Cs, Te, Mo and Ba) were obtained with the two codes (FS + SGPS-SGTE database and OC + extended TBASE).

The modeling of oxidation/reduction of the fuel that takes place during severe accidents relies on a solid solution model for the uranium, plutonium and dissolved FPs (mostly rare earth) already included in the TBASE. The description of the hypo- and hyper-stoichiometric domains of the U-Pu-O system is based on the work of Lindemer and Besmann [28]. The thermodynamic representation of rare earth solubility (La, Y, Gd, Nd, Pm, Ce) is detailed in reference [29]. The data and solubility of Eu is extracted from Dumas [22]. A thorough validation of the the solid solution model on the U-O, U-Pu-O, U-Gd-O, U-La-O, U-Ce-O, U-Eu-O, U-Zr-O systems, on SIMFUELS (Simulated high-burnup nuclear fuel) and on irradiated fuels by comparing the calculated and measured fuel oxygen potential (i.e., $RT \ln p_{O_2}$ with R the gas constant, T, the temperature and p_{O_2} the oxygen partial pressure) is detailed in reference [30]. The assessment of the oxygen partial pressure in the fuel is essential to capture the chemical speciation of FPs during the VERCORS test sequences, as discussed by Riglet-Martial et al. [31]. A more recent thermodynamic database (the Thermodynamic Advanced Fuel International Database or TAF-ID [32]) with up-to-date models for the U-O-FP system, is available to the authors and has been used to double check the calculation of the oxygen potential of the fuel during the VERCORS tests with the TBASE. The higher quality of the solid and liquid phase description likely to form during severe accidents provided by the TAFID (see reference [33]) having a limited impact on the volatile and semi-volatile FP release, the TBASE has been prefered in this work to illustrate the potential of the proposed coupling procedure. It was also of interest to the authors to compare the response of the same database (TBASE) in very different situations, Pellet Cladding Interaction from a previous work [18] and severe accidents (this work).

Overall, a typical thermodynamic equilibrium calculation with OC and the TBASE provides the following information: composition of the gas phase (proportion of each FP in the gas phase), composition of the solid solution phase (proportion of each FP in the fluorite matrix), composition of the noble metal phase (proportion of Mo, Ru and Pd in the phase), concentration in stoichiometric compounds in the fuel, partial oxygen pressure in equilibrium with the fuel.

2 Modeling of fission gas release

It is out of the scope of this paper to propose a mechanistic model for fission gas release where the distribution of fission gases between bubbles, grain faces, edges and pores is described. There are two reasons for that. First, the aim here is to discuss a coupling procedure between gas diffusion and thermochemical equilibrium calculations that can be readily implemented

in a fuel performance code. For demonstrative purpose, a diffusion model on an equivalent spherical grain is sufficient provided it fits well the experimental release kinetics. Second, it is common knowledge that gas bubble migration in the grains in mechanistic models usually depends on the local thermal gradient. In the VERCORS tests, the temperature in the fuel is uniform which generally hinders bubble migration. In the MFPR code, a specific gas bubble migration mechanism related to dislocations had to be implemented to model the release of fission gases in a uniform temperature field [15]. As of today, this mechanism is not available in the MARGARET model of the PLEIADES/ALCYONE fuel performance code.

The simplest model that can be adopted for post-irradiation annealing experiments at high temperature is the equivalent sphere model [34] that gives satisfactory results in most of severe accident codes [11][35]. It relates the fission gas release kinetics to a diffusion process in an equivalent spherical fuel grain. It does not provide any description of the trapping sites that form in irradiated fuels (bubbles, dislocations...). A similar formulation is proposed here for the gas phase including the noble gases and the gases involving chemically-reactive FPs. The overall gas concentration C in a spherical grain of radius r is given by the following equation:

$$\frac{\partial C}{\partial t} = \frac{1}{r^2}\frac{\partial}{\partial r}\left(Dr^2\frac{\partial C}{\partial r}\right) + \frac{\partial S_{FP}}{\partial t} \tag{1}$$

where D is a diffusion coefficient and r the radial position in the sphere. The specificity here is the inclusion of the term $\partial S_{FP}/\partial t$ related to the gases formed from chemically reactive FPs, as calculated from the thermochemical equilibria. We will refer to this term by the name "source term" within this paper. The boundary condition at the spherical grain surface is $C(R,t) = 0$. Instantaneous release of the gas from the fuel is thus assumed when it reaches the grain surface. The diffusion coefficient is conveniently given by the following expression:

$$D(T) = D_0 \times \exp\left(-\frac{Q}{RT}\right) \tag{2}$$

with Q the activation energy and D_0 a constant parameter. With the source term $\partial S_{FP}/\partial t$ and during an annealing test at non constant temperature, the solution of equation 1 requires a numerical solution. A Finite Volume scheme is used to solve equation 1 at each time step.

3 Coupling of fuel thermochemistry and fission gas release

3.1 Short description of a VERCORS test sequence

Before detailing the coupling procedure between fuel thermochemistry and fission gas release, it is necessary to briefly describe a typical test sequence of the VERCORS program undertaken at CEA. To avoid repetition, the two VERCORS 4 and 5 tests that will be simulated in the next part are briefly presented. The test samples consisted of small rodlets (containing 3 fuel pellets) extracted from the same father rod, with a local burnup of 38 GWd/tU. The rodlets were not closed at both ends so that the injected gases in the oven could flow within the rodlets during

the tests. The test sequences included several temperature plateaus, as shown in Figure 2, with slow temperature ramps between them. The experimental sequence began with one or more plateaus at moderate temperature (∼650-750 K) with a constant He flow rate in the furnace. Temperature was then progressively increased till reaching 1500-1550 K and maintained at this level during 30 minutes. At the same time, the gas composition in the furnace was switched to a mixture of H_2/H_2O which led to a complete oxidation of the cladding before the end of the plateau. Temperature was then again increased till reaching a high temperature plateau (2500 K) which was maintained during 30 minutes. The main difference between the VERCORS 4 and 5 tests lies in the thermochemical conditions applied in this last temperature ramp and plateau. During the VERCORS 4 test, the gas composition in the furnace was highly reducing (H_2/He) while that of the VERDON 5 test was highly oxidizing (H_2O only).

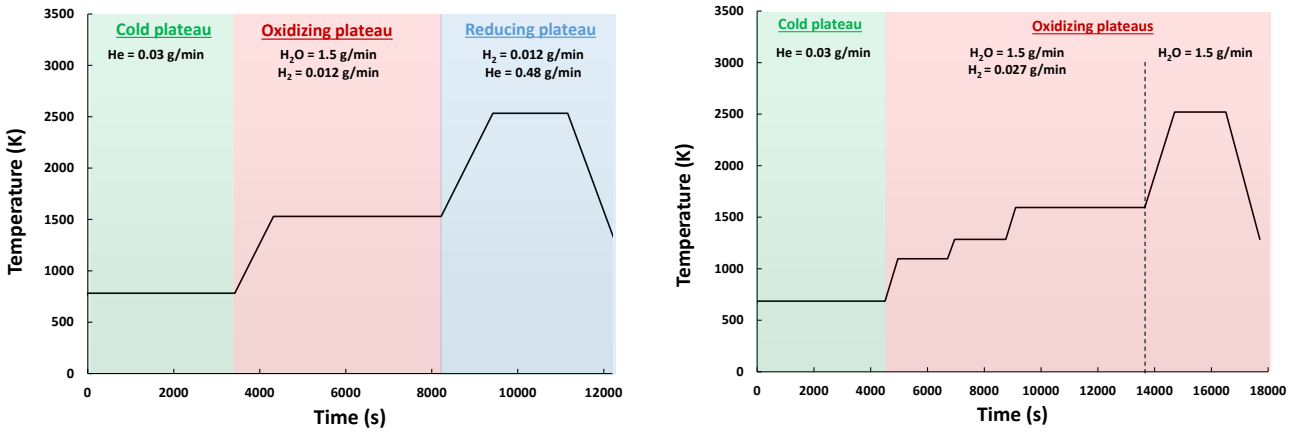

Figure 2: Temperature evolution and injected gas composition during the VERCORS 4 (left) and 5 (right) tests.

As will be discussed in the next parts, the modeling of the injected gases and of their reaction with the fuel and the cladding is not a straightforward matter.

3.2 Coupling between fuel thermochemistry and fission gas release

The simulation of a VERCORS test relies on a time discretization of the sequence. At each time step, the following successive calculations are performed:

- Estimation of the H, O and He content in the furnace from the injected gas composition, the flow rates and the time step,
- Thermochemical equilibrium calculation of the system U-O-FPs plus H-O-He from the injected gases,
- Estimation of the gas content formed in the fuel from the chemically reactive FPs during the time step (source term),

- Solution of the diffusion equation with the source term to estimate the fraction of the total gas content released during the time step,
- Estimation of the amount of each FP released fromt the fuel (concentration in the gas phase times fraction of gas released)
- Update of the FP content in the fuel for the next time step.

Several tests were performed with decreasing time steps in order to check the consistency of the calculations. A time step less or equal to 10 s was found adequate in the simulations of the VERCORS 4 and 5 tests, leading to calculation results independent of the time step.

At this stage, a few points must be emphasized. At each time step, part of the carrier gas does not react with the fuel leading to the formation of water and dihydrogen. Since a constant injected gas flow holds in the furnace, it is assumed that this excess O-H will be taken away by the carrier gas. It is therefore not available at the next time step. The O and H that react with the FPs in the fuel can lead to the formation or not of gas compounds. The release of the latter from the fuel depends on the diffusion controlled release rate of the bulk of the gas phase.

A single thermochemical equilibrium calculation is performed at each time step assuming that all FPs are readily available in the fuel for reaction. This is a major hypothesis that is generally not adopted in severe accidents codes where chemical reaction between FPs is usually assumed to take place at the grain faces due to the important FP concentration in gas bubbles at this location [15]. The non differentiation of intra- and inter-granular local thermochemical equilibria in our coupling scheme is consistent with the recent analysis by EPMA (Electron Probe Micro-Analysis) and SIMS (Secondary Ion Mass Spectrometry) of the content of an intra-granular bubble formed at the center of a fuel pellet during a power ramp [36]. It clearly showed the co-existence of 4 different precipitates in the bubble formed by the combination of Cs, I, Te, Ba for two of them and Mo, Pd, Ru, Rh for the other two. The authors of this study attribute these observations to the possible coalescence of 4 different bubbles which each contained a single precipitate. The other observation of importance is the non homogeneous concentration of FPs within the fuel grains. These findings imply that the FPs are likely to gather rapidly during irradiation in intra-granular bubbles filled with noble gas. Hence the hypothesis considered in our work of a single thermochemical equilibrium calculation involving all the FPs remaining at each time step in the fuel.

The FPs released at each time step are estimated from the fraction of gas released times the FP concentrations in the gas phase. The fraction of gas released is defined here as the instantaneous gas fraction. In other words, the denominator is not the initial gas content but the remaining gas content.

The importance of the source term can be explained as follows. In some VERCORS tests, the release of noble gases proceeds more rapidly than that of other FPs. At some point, the release of noble gases may be total. If the source term is not included in the diffusion equation, this may result in the total suppression of other FPs releases even if the FPs form gas compounds in the fuel. The inclusion of the gases formed from chemically reactive FPs in the gas diffusion equation is also consistent with the previously discussed observations of precipitates in an intra-granular bubble.

The cladding is not included in the present coupling scheme in spite of experimental observations that showed its importance in the immobilization of a small part of some FPs released from the fuel, in particular Ba during the VERCORS 5 sequence, as shown from post-test gamma tomography [5][37][33]. In practice, the introduction of all or part of the cladding in the thermochemical calculations is possible and will be one of the points tackled in the discussion. At temperatures close to the fuel melting temperature, there is also strong evidence that part of the oxidized cladding reacts with the fuel and forms a mixed (U,Zr)O_{2-x} phase [10][33]. This aspect is out of the scope of the present work.

4 Results

4.1 Mesh and gas diffusion parameters

Calculations in this work were undertaken within the fuel performance code ALCYONE where the OC thermochemical software is fully operational and can be called at each node and time step of a fuel simulation [21]. In the proposed application to the VERCORS 4 and 5 tests intended to test the thermochemical - fission gas diffusion coupling, a simplified mesh of the fuel pellets was considered with only one element spanning over the pellet radius. The fuel burnup and FP peaked profiles at the pellet periphery are thus not taken into account. The average burnup of the fuel pellet is considered in the simulations (38 GWd/tU).

The temperature histories of the VERCORS 4 and 5 tests were applied to the same pre-irradiated fuel sample as explained above. The main difference in the two tests lies in the injected gas composition during the last temperature ramp and plateau. The aim of the simulations is therefore to capture the consequences of these differing injected gas composition on the FP release at high temperature.

To make sure that the differences in FP release stems only from the thermochemical equilibrium calculations, the same parameters were used for the gas diffusion model in the two tests.

To fit the parameters, the ^{133}Xe release rates measured on-line have been used, as shown in Figure 3.

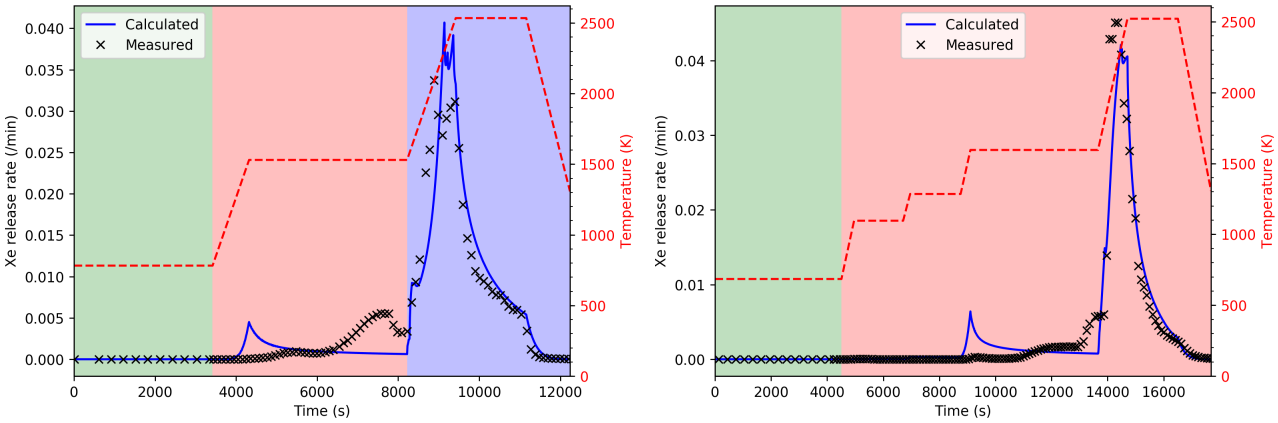

Figure 3: Measured and calculated release rates of ^{133}Xe during the VERCORS 4 (left) and VERCORS 5 (right) tests. The second Y-scale refers to the temperature evolution during the tests.

Considering an average grain radius of 5 μm, and the activation energy identified by Booth in the first presentation of the equivalent sphere model, i.e., $Q = 188$ kJ/mol [34], the fitting of the Xe release kinetics relies on a single parameter, $D_0 = 1.09 \times 10^{-11}$ m^2/s. Obviously, this very simple approach gives a good estimation of the Xe release kinetics during the tests. The main peak of ^{133}Xe that is seen during the last temperature ramp is well captured by the model. The progressive increase of the release rate that is observed during the oxidation temperature plateau in both tests is however not reproduced by the model. The shape of the experimental release rate is not consistent with a diffusion mechanism at constant temperature that leads to an exponentiel decay of the release rate after an initial peak. It is inferred that the oxidation-induced failure of the cladding during this plateau leads to a loss of the mechanical constraint on the pellet that probably eases the release of fission gases after this event. It may also be possible that the Xe release has been hindered before clad failure.

Note that ^{133}Xe is a short-lived FP that was generated during the re-irradiation in the SILOE reactor. The VERCORS 4 and the VERCORS 5 tests were re-irradiated during 7 days at a power of 18 W/cm for the VERCORS 4 test and 13 W/cm for the VERCORS 5 test. ^{133}Xe release rate is therefore representative of the intra-granular diffusion rate of noble gases. It does not account for inter-granular fission gases that might have accumulated during the irradiation of the father rod in reactor prior to the tests.

The importance of the source term $\partial S_{FP}/\partial t$ with respect to the release of noble gases (Xe) is illustrated in Figure 4. The graph on the left gives the calculated versus measured cumulated

release of Xe during the VERCORS 4 test. The graph on the right gives the evolution of the gas contribution due to the source term divided by the initial Xe inventory (in percentage).

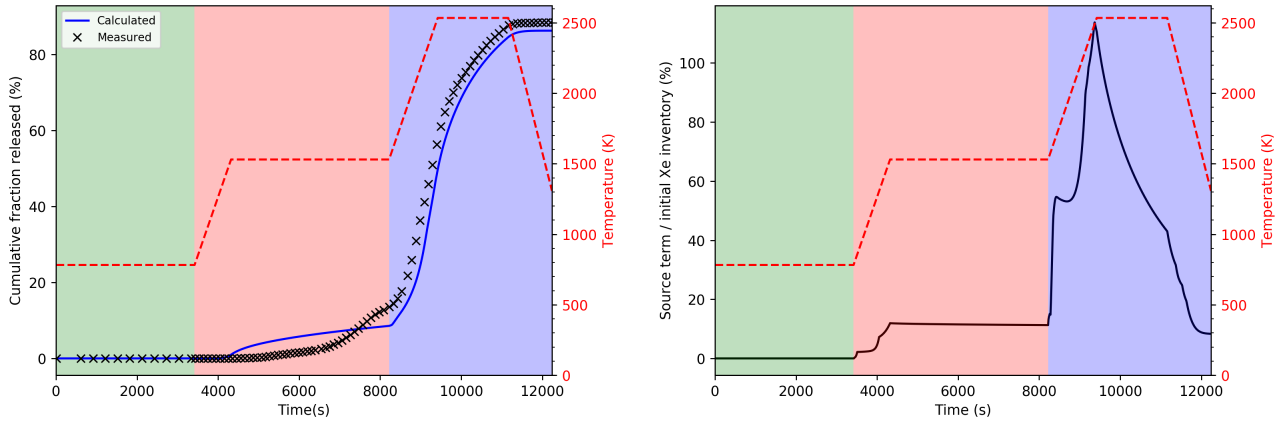

Figure 4: Calculated versus measured ^{133}Xe release (left graph) and gas contribution from the source term evolution (right graph) during the VERCORS 4 test. The second Y-scale refers to the temperature evolution during the test.

As can be seen from the left graph, the diffusion model leads to a good fit of the released fraction of Xe, except during the oxidation plateau for the reasons discussed before (possible impact of the cladding). The right graph shows that the contribution of the source term (i.e., gas content in the fuel related to the chemically reactive FPs) to the total gas content (including noble gases) is non negligible and can be of the same order than noble gases, in particular during the high temperature phase of the VERCORS 4 test where gas compounds are likely to form.

4.2 Oxidation/reduction of the fuel

The oxidation/reduction of the fuel during the VERCORS test sequences is a direct output of the thermochemical equilibrium calculations that include a solid solution model for the U-O-FPs system. Compared to other severe accident codes, there is no specific oxidation kinetics model in the simulations. Thermodynamic equilibrium of the fuel with the injected gases in the furnace is assumed at all time. Of course, this might prove a strong hypothesis at moderate temperatures (up to 1250 K) but is considered valid after the oxidation plateau is reached.

Figure 5 shows the evolution of the calculated oxygen potential of the fuel during the VERCORS 4 and 5 tests.

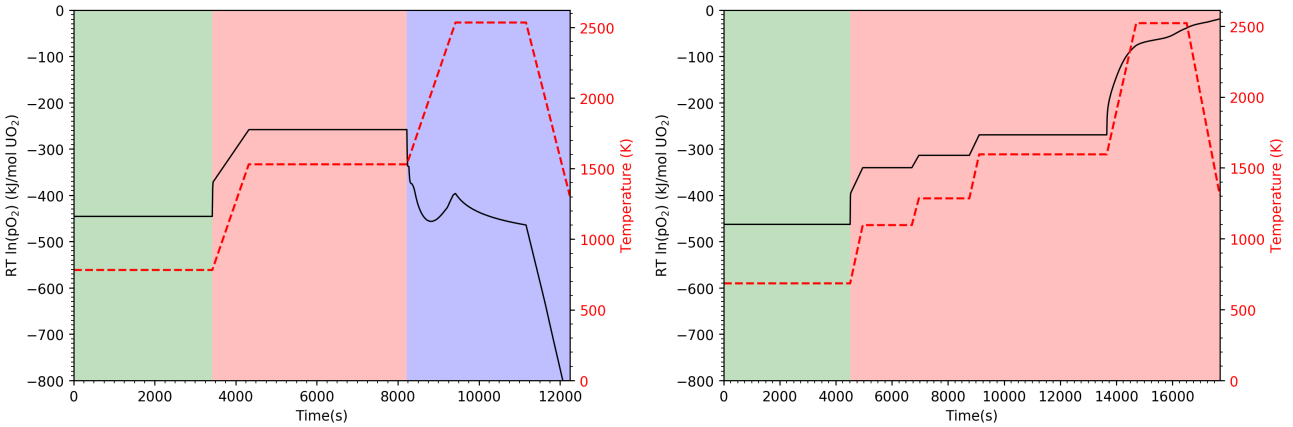

Figure 5: Calculated oxygen potentials during the VERCORS 4 (left) and VERCORS 5 (right) tests. The second Y-scale refers to the temperature evolution during the tests.

Before the oxidation plateau, the oxygen potential follows the temperature evolution. A sudden increase of the potential can be seen at the end of the first temperature plateau in the VERCORS 4 and 5 tests. It is related to the change of the injected gas composition from He to a mixture of H_2O and H_2. In spite of small differences in the mole ratio of H_2O and H_2 between the VERCORS 4 and 5 tests, the oxygen potentials calculated on the oxidation plateau are close (around -270 kJ/mol). As discussed in reference [27], the oxygen potential at this point is mostly driven by the composition of the injected gas, that is the ratio H_2O/H_2. Actually, the release of H_2 resulting from the oxidation of the clad between 1000 K and 1500 K is likely to modify to a greater or lesser degree the O_2 partial pressure at equilibrium. However, no significant change in the FP releases is expected in this low temperature range. Therefore, this issue was not considered in the present study. After the oxidation plateau, the oxygen potentials in the two tests start to diverge:

- In the VERCORS 4 test, the H_2O from the H_2/H_2O mixture is removed and replaced by He while the H_2 flow remains the same. Under these highly reducing conditions, the O_2 partial pressure, which is no longer buffered, is likely to undergo large variations depending on the residual H_2O content in the furnace. This may have a significant impact on gaseous FP releases as discussed later on in section 5. The oxygen potential curve shown in the high temperature range of Figure 5 (left graph) refers specifically to the most reducing case when the H_2O content in the gas is null. In those limiting conditions, the oxygen potential is driven in-situ by the irradiated fuel itself, which results in a very sharp decrease somewhat limited in magnitude by the simultaneous increase of temperature. The oxygen potential finally stabilizes around -450 kJ/mol before decreasing sharply during the cooling down of the furnace.

- A very different picture holds during the last part of the VERDON 5 test. The conservation of H_2O in the carrier gas during the high temperature step of the test leads to a fast increase of the oxygen potential of the fuel which exceeds -100 kJ/mol before cooling

down. In fact, under these highly oxidising atmosphere, the fuel-cladding interaction giving rise to a (U, Zr)O_{2+x} solid solution, and the emerging degradation/sublimation of the fuel make the thermochemical description of the system more complex [38]. In addition, impurities or residual H_2 in the carrier gas may also affect the equilibrium O_2 partial pressure, which may have a significant impact on gaseous FP releases as discussed later on in section 5. Thus, in the high temperature range, the oxygen potential may be driven by either the carrier gas or the fuel material, depending on the test conditions (H_2O flow rate, residual H_2, Zr content). The oxygen potential curve shown in the high temperature range of Figure 5 (right graph) refers specifically to the oxidising limit case, when the H_2 content in the carrier gas entering the furnace is null and no Zr coming from the cladding is incorporated into the fuel.

These calculation results show the tremendous impact of the actual test conditions (cladding interaction and atmosphere) on the oxygen partial pressure at equilibrium, and consequently on the O/M ratio of the fuel. In fact, starting from an initially stoichiometric fuel (O/M = 2), the O/M ratios are very similar in the two tests until the end of the oxidation plateau (where O/M $\sim$ 2.005). However, in the high temperature range, the O/M ratios undergo huge variations (1.98 < O/M < 2.12) depending on the test conditions.

4.3 Release kinetics and speciation of volatile FPs

Figure 6 presents the calculated and measured fractions of iodine released from the fuel during the VERCORS 4 and 5 tests.

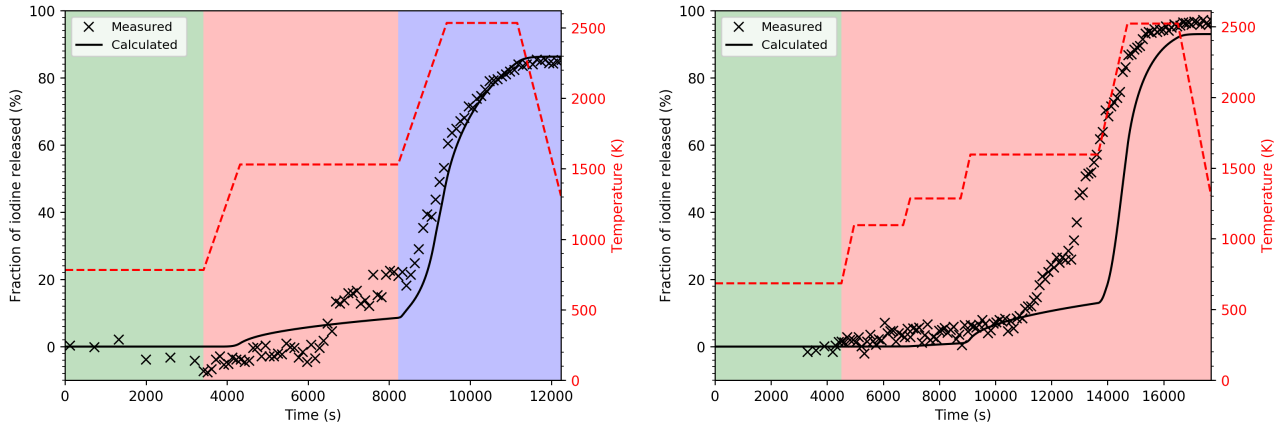

Figure 6: Calculated and measured fractions of iodine released during the VERCORS 4 (left) and 5 (right) tests. The second Y-scale refers to the temperature evolution during the tests

Overall, a very good agreement between calculations and measures is obtained during both tests. Small differences appear during the oxidation plateau. They are due to the differences in fission gas release that were described in part 4.1 and attributed to the delayed clad failure. The fractions of iodine released at the end of the tests (around 80%) are also well estimated.

The chemical speciation of iodine in the fuel during the VERCORS 4 test is presented in Figure 7.

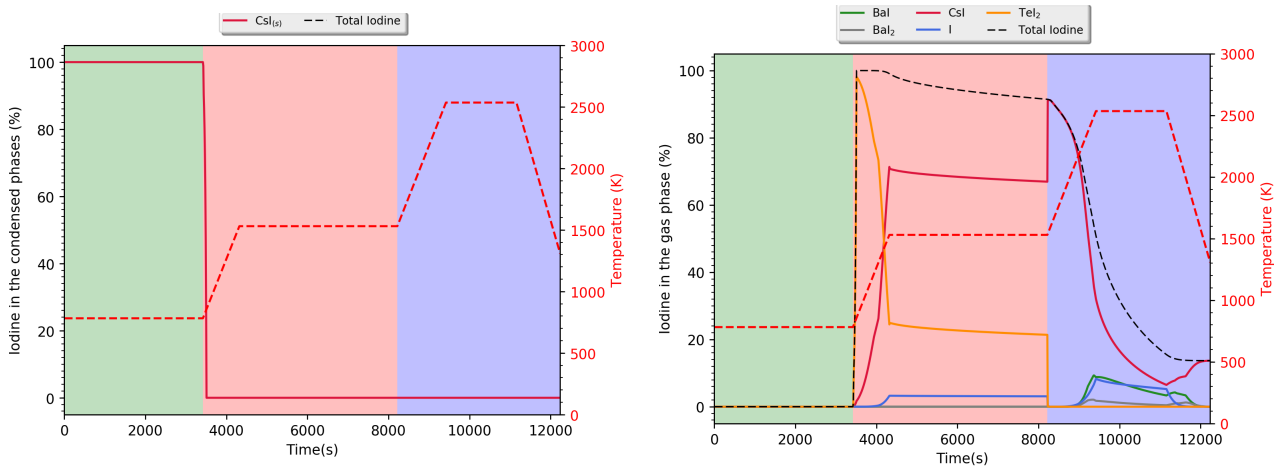

Figure 7: Chemical speciation of iodine in the condensed phases (left) and in the gas phase (right) during the VERCORS 4 test. The second Y-scale refers to the temperature evolution during the test

The left graph of Figure 7 shows the speciation of iodine in the fuel, gas phase excluded. Below 700 K and during the He injection, all iodine reacts with caesium (abundant FP) and forms $CsI_{(s)}$. With the increase of temperature and the change in the carrier gas composition to a mixture of H_2 and H_2O, all iodine becomes gaseous. The speciation of iodine in the gas phase is presented in the right graph of Figure 7. The change of the carrier gas composition leads to the formation of a massive quantity of $TeI_{2(g)}$ (including 100% of iodine). Then $TeI_{2(g)}$ is progressively dissociated with temperature increase and the freed iodine reacts with caesium to form $CsI_{(g)}$. During the oxidising plateau, there is around 1/3 of the iodine in $TeI_{2(g)}$ and 2/3 in $CsI_{(g)}$ (100% of iodine is in the gas phase). There are also traces of $I_{(g)}$ and $BaI_{x(g)}$ $(x = 1, 2)$. During the last phase of the VERCORS 4 test, the increase of the fission gas release rate with temperature and the availability of iodine in the gas phase leads to a fast release of iodine (85% is released during the last temperature plateau). Total release is not reached because of the limited duration of the high temperature plateau. A very similar chemical speciation is obtained for iodine during the VERCORS 5 test and is therefore not presented in specific figures.

The behavior of tellurium during the VERCORS 4 and 5 tests is similar to that of iodine, as shown in Figure 8. The measured tellurium does not appear at the end of the test since its detection by online gamma spectrometry is complicated. However the final released fraction is known thanks to the post-test measures made on each part of the loop (∼100%).

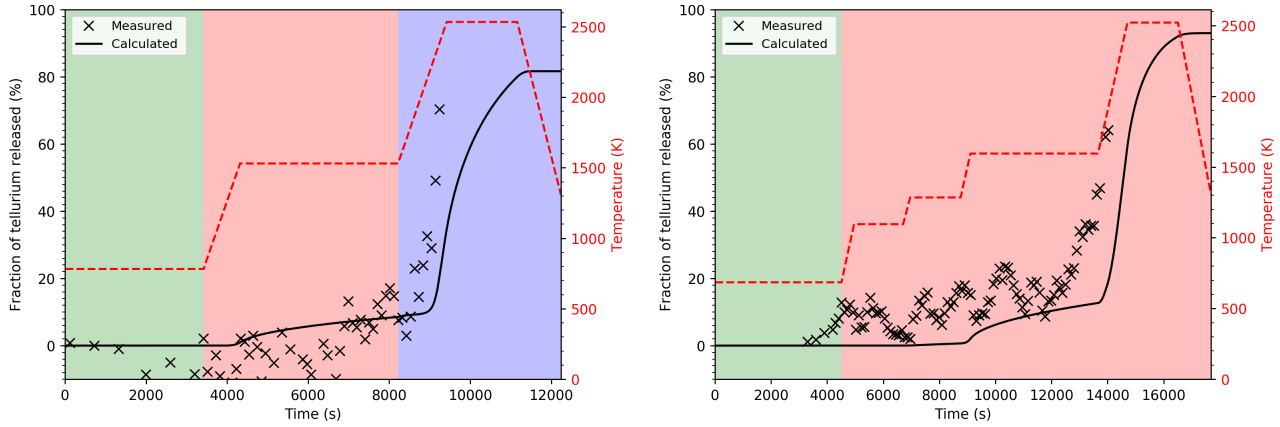

Figure 8: Calculated and measured fractions of tellurium released during the VERCORS 4 (left) and 5 (right) tests. The second Y-scale refers to the temperature evolution during the tests

The final released fractions are slightly underestimated in both tests since the gas transport model gives a slightly underestimation in the ^{133}Xe release but the calculated release kinetics compare well with experimental measures. The chemical speciation of tellurium during the VERCORS 4 tests is presented in figure 9.

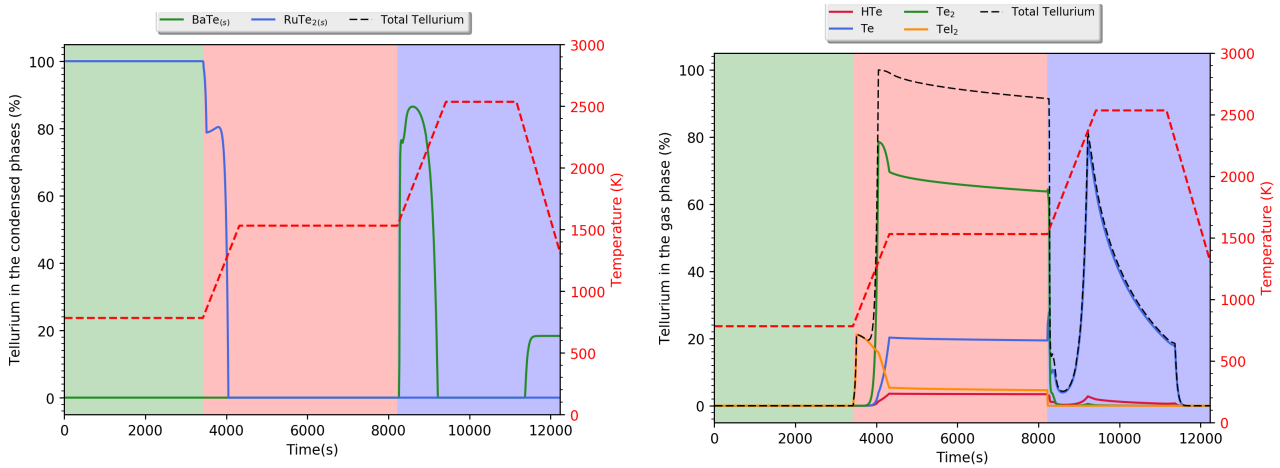

Figure 9: Chemical speciation of tellurium in the condensed phases (left) and in the gas phase (right) during the VERCORS 4 test. The second Y-scale (on the right) refers to the temperature evolution during the test

The left graph of Figure 9 shows that tellurium forms $RuTe_{2(s)}$ until the injected gas composition is changed to oxidizing conditions. Tellurium first combines with iodine to form $TeI_{2(g)}$ ($\sim$20% of the total tellurium available in the fuel). With increasing temperature, all tellurium progressively forms gaseous compounds, $Te_{(g)}$ and $Te_{2(g)}$ for the major part (80-90%) and $HTe_{(g)}$ for less than 5%. When the injected gas is switched back to He, tellurium precipitates as $BaTe_{(s)}$. When the temperature reaches $\sim$1900 K, sublimation of $BaTe_{(s)}$ into $Te_{(g)}$

(and $HTe_{(g)}$ for a small quantity) takes place. The coupling with the fission gas release model and the availability of Te in the gas phase leads to a fast release of tellurium characterized by the decrease in the total tellurium percentage in the gas phase (black dashed line). Note that the release of tellurium is slightly shifted in time when compared to iodine. At the end of the test, with the temperature drop in the fuel, the remaining tellurium precipitates as $BaTe_{(s)}$. A very similar chemical speciation in the gas phase is obtained during the VERCORS 5 test and is not presented for this reason. The third FP of interest within the volatile FPs is caesium. Since its chemical speciation in the fuel is dependent on Mo and Ba, it will be presented in the section 4.4 devoted to semi-volatile FPs.

4.4 Release kinetics and speciation of semi-volatile FPs

Figure 10 shows the released fractions of caesium during the VERCORS 4 and 5 tests.

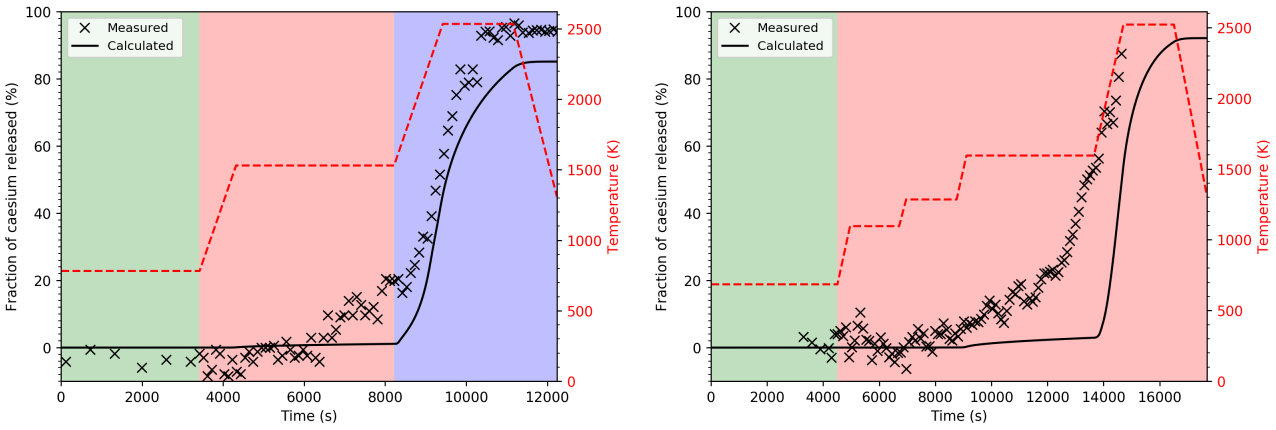

Figure 10: Calculated and measured fractions of caesium released during the VERCORS 4 (left) and 5 (right) tests. The second Y-scale refers to the temperature evolution during the tests

As can be seen, there is a general agreement between calculated and measured caesium release curves in both VERCORS tests. The simulations end with a slightly underestimated fraction of caesium released (∼85% for ∼95% measured). The difference is mostly due to the behavior of caesium during the oxidation plateaus where nearly no caesium is released in the simulation while measures indicate that between 0% and 20% of the total caesium left the fuel. This can be explained by the chemical speciation of caesium during the VERCORS 4 and 5 tests, as shown in Figure 11.

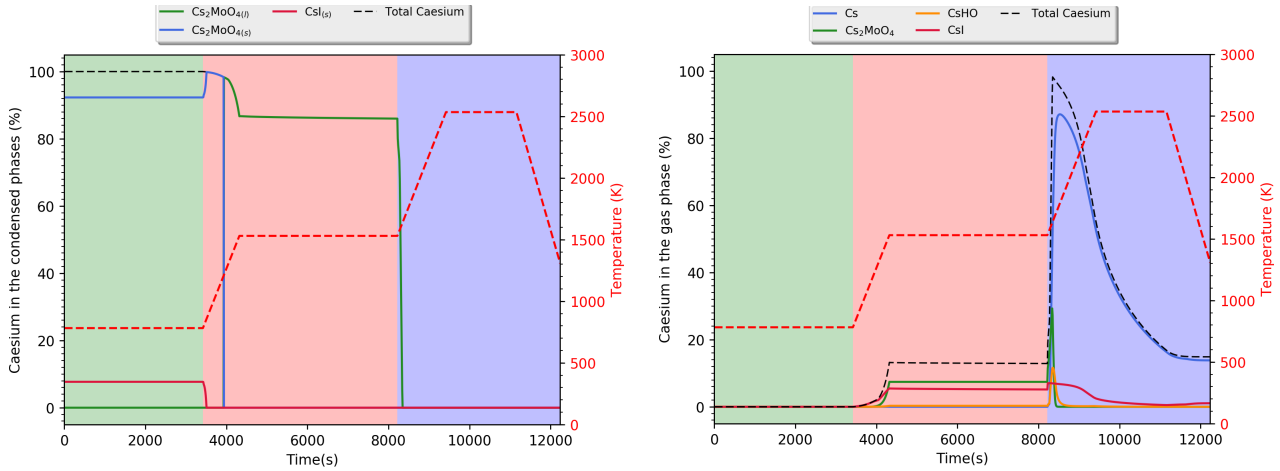

Figure 11: Chemical speciation of caesium in the condensed phases (left) and in the gas phase (right) during the VERCORS 4 test. The second Y-scale (on the right) refers to the temperature evolution during the test

Considering the VERCORS 4 test, before the oxidation plateau, caesium is predominantly associated with molybdenum in $Cs_2MoO_{4(s)}$ (∼90% of the total quantity of Cs) and with iodine in $CsI_{(s)}$ (∼10% of the total quantity of Cs). Around 1200 K, 85% of $Cs_2MoO_{4(s)}$ becomes liquid ($Cs_2MoO_{4(l)}$) and the remaining fraction forms gaseous compounds ($Cs_2MoO_{4(g)}$, $CsI_{(g)}$ and $CsHO_{(g)}$ in decreasing order of importance). The speciation does not change during the oxidation temperature plateau. Compared to the 100% iodine and tellurium in the gas phase during the oxidation plateau, this 15% caesium in the gas phase is not sufficient to induce a significant release of this FP. This explains the difference with the two other volatile FPs. After the oxidation plateau, as soon as the carrier gas composition is changed, reduction of $Cs_2MoO_{4(l)}$ according to the reaction $Cs_2MoO_{4(l)} = 2Cs_{(g)} + Mo_{(s)} + 2O_2$ leads to the formation of a huge quantity of $Cs_{(g)}$ (100% of the caesium in the fuel). Combined with the fast gas diffusion triggered by temperature increase, it explains the release of 85% of the caesium during this last phase.

For the VERCORS 5 test, the picture is a bit different during the last phase of the test due to the oxidizing gas environment that holds. Sublimation of $Cs_2MoO_{4(l)}$ leads to the formation of $Cs_2MoO_{4(g)}$ and $CsHO_{(g)}$ to a lesser extent (see Figure 11). As in VERCORS 4, all caesium available in the fuel is in the gas phase which explains the fast release during the temperature ramp and plateau. The caesium release rate is thus similar to that of VERCORS 4 but the chemical speciation during the last phase of the test is totally different and very sensitive to the injected gas composition.

Figure 12 shows the fraction of molybdenum released during the VERCORS 4 and 5 tests.

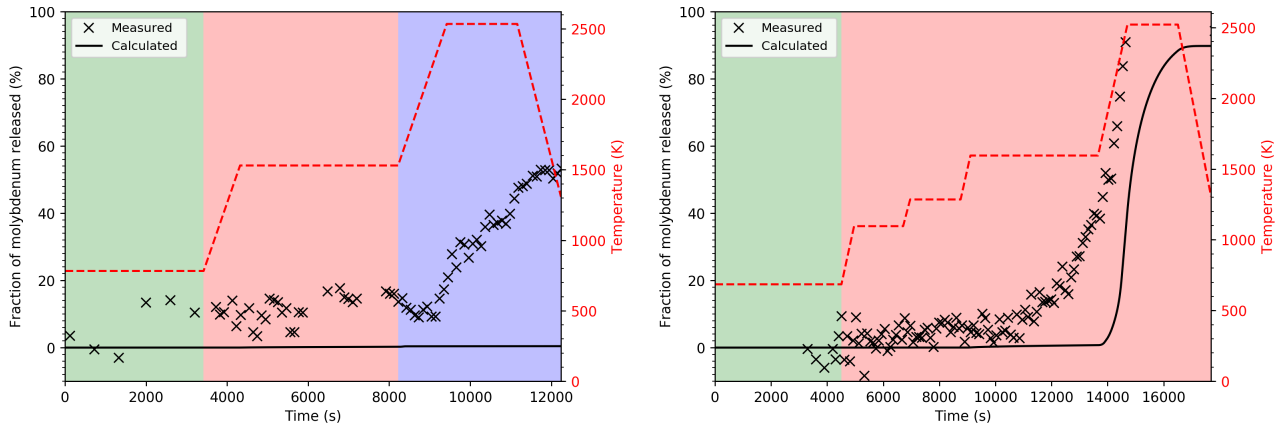

Figure 12: Calculated and measured fractions of molybdenum released during the VERCORS 4 (left) and 5 (right) tests. The second Y-scale refers to the temperature evolution during the tests

Contrary to the volatile FPs, the behavior of molybdenum during the VERCORS 4 and 5 tests is different. A smaller fraction of molybdenum has been released at the end of the VERCORS 4 test (∼60%) compared to the VERCORS 5 test (∼95%). This trend is recovered in the simulations but the difference in molybdenum release is exacerbated. While the calculated molybdenum release reaches 90% at the end of the VERCORS 5 test, it is almost zero at the end of the VERCORS 4 test. Furthermore, as for caesium, the 20% molybdenum release during the oxidation plateau is not recovered in the simulations. These results can be explained by the chemical speciation of molybdenum presented in Figure 13 for the two tests.

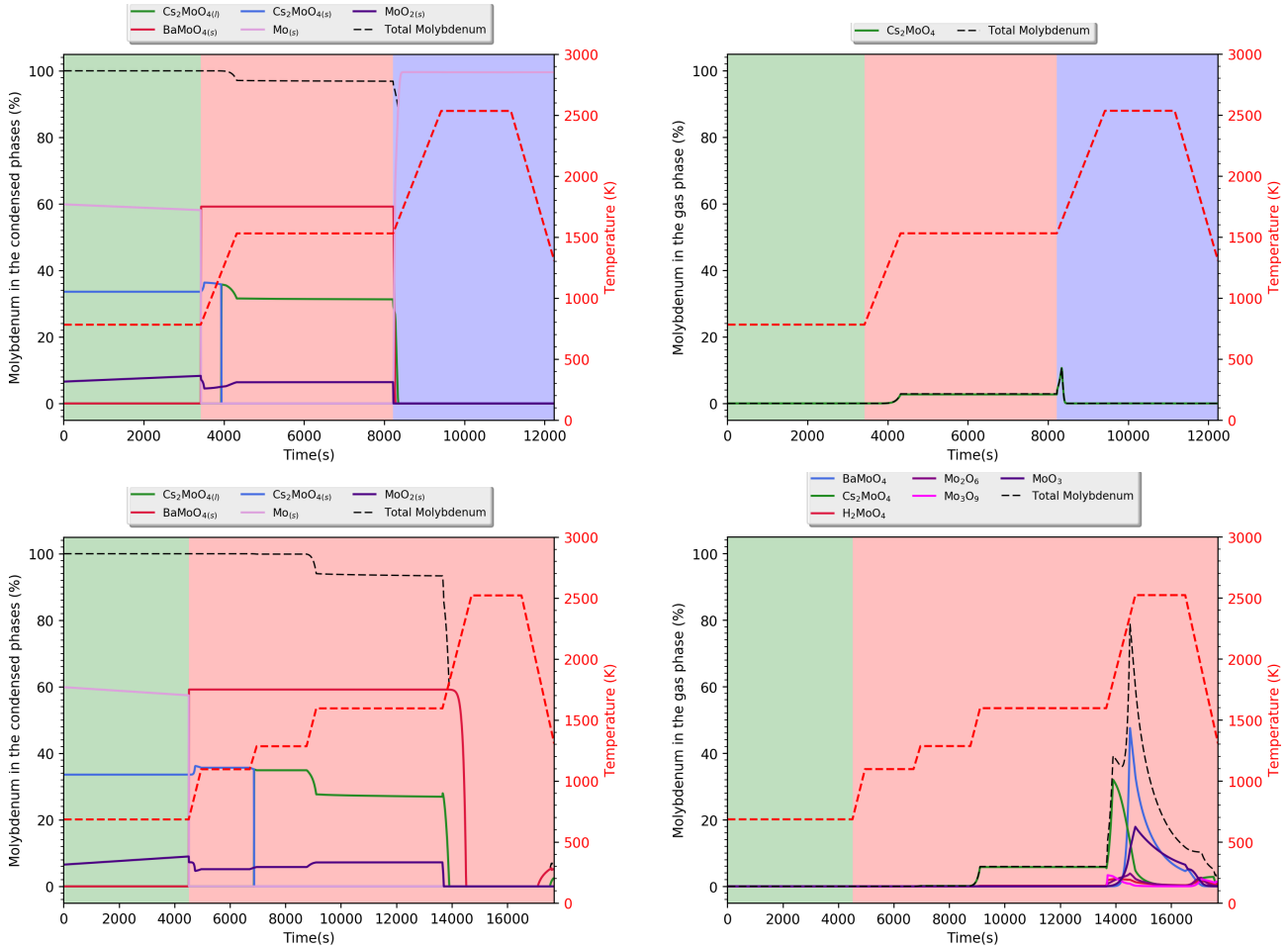

Figure 13: Chemical speciation of molybdenum in the condensed phases (left) and in the gas phase (right) during the VERCORS 4 (top) and 5 (bottom) tests. The second Y-scale refers to the temperature evolution during the test

In the first phase of the test, the external conditions are very close to those taking place in a reactor (rod full of He). According to our simulations, the fuel is nearly stoichiometric during this phase. As expected by comparison to in-reactor conditions [39], molybdenum is mostly found in $Mo_{(s)}$, $MoO_{2(s)}$ and $Cs_2MoO_{4(s)}$. When the gas mixture is switched to H_2O/H_2, metallic molybdenum $Mo_{(s)}$ combines with barium and oxygen to form $BaMoO_{4(s)}$ ($\sim$60% of the total molybdenum content in the fuel). At around 1200 K, caesium molybdate $Cs_2MoO_{4(s)}$ becomes liquid. Only a small fraction of molybdenum (less than 10%) is gaseous during the oxidation temperature plateau ($Cs_2MoO_{4(g)}$). As for caesium, this gaseous fraction is too small to lead a significant release of molybdenum during this plateau.

In the high temperature phase of the VERCORS 4 test where the gas composition in the furnace does not include H_2O anymore (reducing conditions), the molybdenum precipitates entirely as $Mo_{(s)}$. Thus, there is no molybdenum in the gas phase which explains the quasi-

zero molybdenum release at the end of the test. On the contrary, during the VERCORS 5 sequence, the conservation of H_2O in the injected gas (oxidizing conditions) leads to the total sublimation of the condensed phases observed during the oxidation plateau. During the last temperature ramp and plateau, the gas phase includes two molybdates ($Cs_2MoO_{4(g)}$ first then $BaMoO4_{(g)}$), three molybdenum oxydes ($MoO_{3(g)}$, $Mo_2O_{6(g)}$, $Mo_3O_{9(g)}$) and $H_2MoO_{4(g)}$. All the molybdenum in the fuel being in the gas phase, the fraction released increases rapidly and reaches 90% at the end of the test, in good agreement with the measures. The release of Mo observed in the VERCORS 4 test is not in agreement with the simulation, which suggests some gaps or inconsistencies in the database, and/or some inadequate redox conditions applied to the fuel. This point will be discussed in the next section.

Figure 14 gives the calculated and measured evolution of the barium released during the VERCORS 4 and 5 tests.

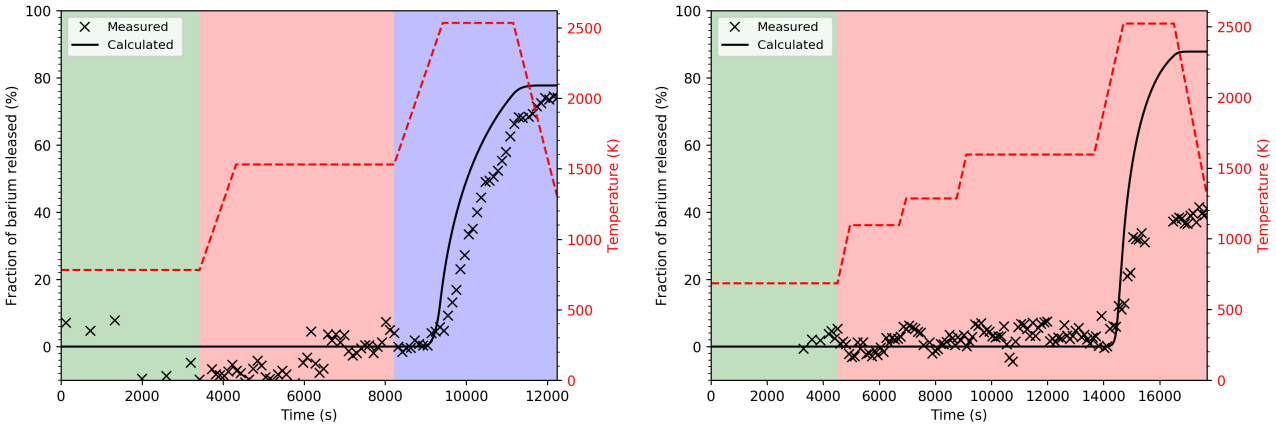

Figure 14: Calculated and measured fractions of barium released during the VERCORS 4 (left) and 5 (right) tests. The second Y-scale refers to the temperature evolution during the tests

The temperature at which barium release begins during the two tests is very well assessed (after the oxidation plateau). The kinetics are also well estimated in the VERCORS 4 simulation. The fraction of barium released at the end of this test is very close to the measure by gamma spectrometry (∼75%). The agreement is less good in the case of the VERCORS 5 test where the simulation overestimates the final release by a factor 2 (∼90% for ∼40% measured). Since the fission gas diffusion model is the same, these results are only a consequence of the chemical speciation of barium in the fuel. Details on the condensed and the gas phases during the simulations are given in Figure 15.

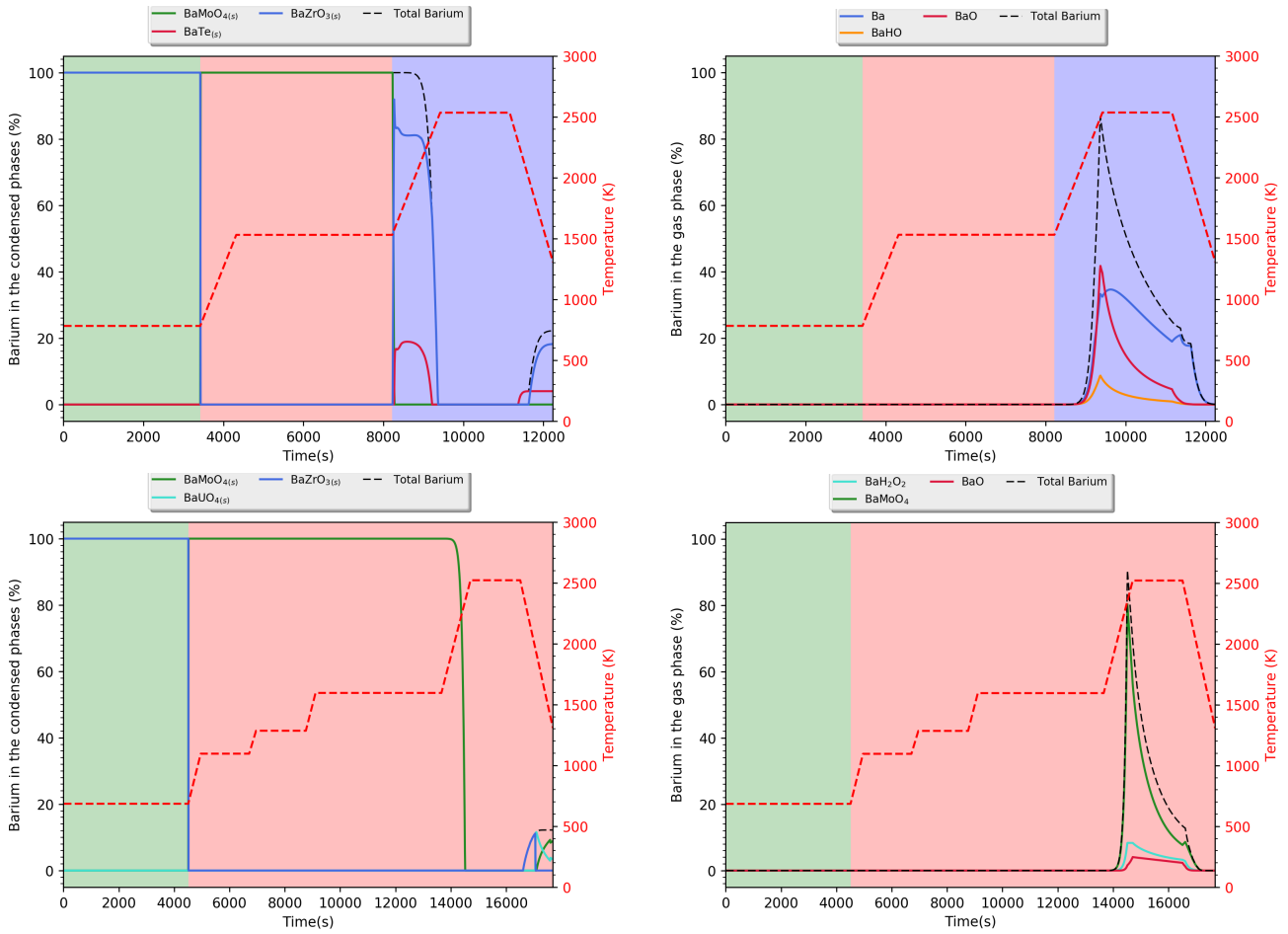

Figure 15: Chemical speciation of barium in the condensed phases (left) and in the gas phase (right) during the VERCORS 4 (top) and 5 (bottom) tests. The second Y-scale refers to the temperature evolution during the test

During the first part of the VERCORS 4 and 5 tests (He carrier gas), barium is mostly found associated with Zr ($BaZrO_{3(s)}$). When the H_2O and H_2 are introduced, barium combines with molybdenum to form $BaMoO_{4(s)}$. During the oxidation temperature plateau, no barium is found in the gas phase which explains the zero release at this stage. In the VERCORS 4 simulation and during the last temperature ramp (reducing conditions), $BaMoO_{4(s)}$ is first converted in into $BaTe_{(s)}$ and $BaZrO_{3(s)}$. Sublimation of these two condensed phases takes place at around 2300 K, leading to a very high fraction of barium in the gas phase (distributed among $Ba_{(g)}$, $BaO_{(g)}$ and $BaHO_{(g)}$, by decreasing order of importance). The delayed sublimation of barium with respect to caesium explains the lower released fraction at the end of the VERCORS 4 test. Sublimation of all the $BaMoO_{4(s)}$ also takes place at around 2300 K during the VERCORS 5 test oxidizing conditions. At this stage, all the barium is found in the gas phase, with a clear predominance of $BaMoO_{4(g)}$ and small quantities of $BaH_2O_{2(g)}$ and $BaO_{(g)}$. This explains the high release of barium during the VERCORS 5 simulation.

These results show the interdependence of the Cs, Mo and Ba release in relative contradiction with the usual classification of caesium in the volatile fission products with no impact of the external conditions. The discrepancies between the measured molybdenum and barium releases and the simulations suggest some inconsistencies in the thermodynamic data, and/or in the redox conditions applied to the fuel. This point is discussed in the next section.

5 Discussion

5.1 Caesium and molybdenum

The estimations of the FP release during the VERCORS 4 and 5 tests presented in this paper rely on a very straightforward coupling between gas diffusion and FP thermochemistry. The gas diffusion model is also in its conception very simple since it does not describe the complex mechanisms at hand in irradiated fuels but considers the diffusion of the total gas phase within fuel grains as a single process. The complexity lies in the thermochemical equilibrium calculations that define the oxygen potential, the O/M ratio, the gas phase composition and the condensed phases evolution in the fuel during the tests. Overall, this coupling scheme leads to very good estimations of iodine, tellurium and caesium release kinetics mainly because the bulk of these FPs is found in the gas phase and readily available for release from the fuel when temperature increases. The chemical speciation of caesium differs in the two VERCORS tests showing it is a function of the applied redox conditions. However, it leads to identical releases at the end of the tests because 100% of caesium is found in the gas phase in both cases, as for iodine and tellurium. An underestimation of caesium release is however visible during the oxidation temperature plateau and will be discussed hereafter. Caesium speciation is strongly related to that of molybdenum (formation of $Cs_2MoO_{4(s,l,g)}$) and should thus not be analyzed independently. Molybdenum release during the VERCORS 5 test (oxidizing conditions) is well assessed by the simulation set apart during the oxidation temperature plateau where the release is underestimated. Since $Cs_2MoO_{4(g)}$ is the main gaseous species found during this phase, the reason for this poor estimation is the same as for caesium (as discussed hereafter).

In their analysis of the VERCORS/VERDON tests, Riglet-Martial et al. [31] pointed out that the molybdenum over caesium release fractions %Mo(t)/%Cs(t) during the oxidation temperature plateau was close to 2/3, which would be consistent with an overall stoichiometry of type $Cs_2Mo_2O_7$ (caesium dimolybdate) and not Cs_2MoO_4 (caesium (mono)molybdate). As $Cs_2Mo_2O_7$ may also be written as $Cs_2MoO_4 + MoO_3$, this stoichiometry is theoretically consistent with either a single gaseous species $Cs_2Mo_2O_7$ or two concomitant Cs_2MoO_4 and $(MoO_3)_n$ gaseous species, in proportion Cs/Mo=1. In fact, it is hard to decide between the two descriptions, in the current state of knowledge. On one hand, the gaseous species $Cs_2Mo_2O_7$ has never been identified, nor characterized directly, which nevertheless does not prove its nonexistence. On the other hand, Do et al. [40] concluded from their observations on vaporization and deposition of caesium dimolybdate, that the later unequivocally vaporizes as $Cs_2Mo_2O_{7(g)}$

rather than decomposes to $Cs_2MoO_{4(g)}$ and $Mo_nO_{3n(g)}$. In the simulations with the TAF-ID described in [33], a Cs/Mo = 1 proportion is never obtained even if the actual Mo activity in the Mo-Ru-Pd-Rh alloys is taken into account instead of that of the pure Mo compound (as assumed in the present study). Nevertheless, the discrepancies might come from gaps or inconsistencies in the thermodynamic description of the Mo-O gas phase, which is known for its high complexity. In fact, this discussion poses the issue of the quality (still insufficient) of the Thermodynamic Databases at hand, for some key chemical systems (such as Cs-Mo-O) that are essential for the irradiated fuel behaviour. Anyway, in order to evaluate the potential benefit of the hypothetic compound $Cs_2Mo_2O_{7(g)}$ in the simulations of the VERCORS tests, the thermodynamic functions for the solid, liquid and gaseous compounds of $Cs_2Mo_2O_7$ were assessed from the recently published studies [40][41] [42] and added to the current thermodynamic database. The assessment calculations (performed in our group) is out of the scope of the present paper. Recalculation of the caesium and molybdenum releases during the VERCORS 4 test including $Cs_2Mo_2O_{7(s,l,g)}$ are presented in Figure 16.

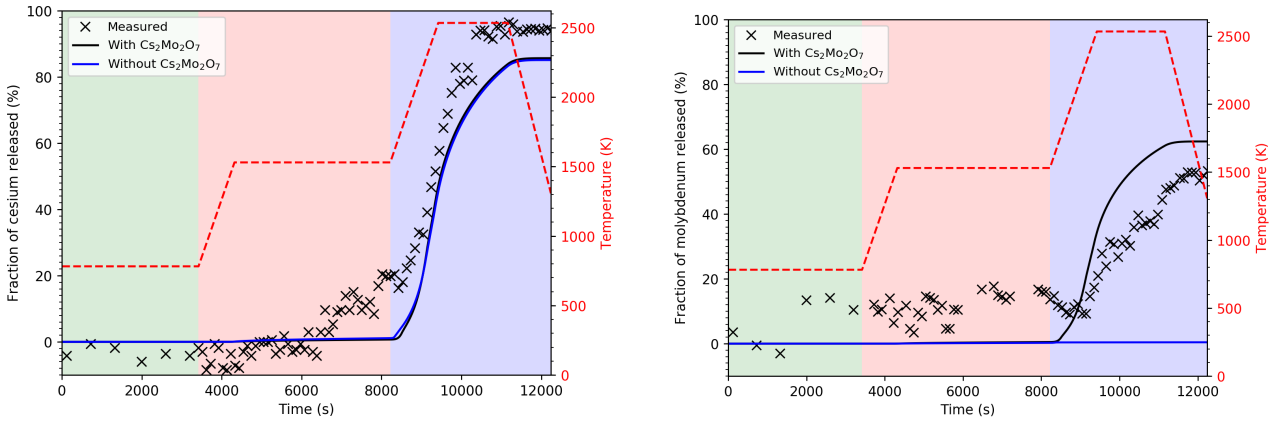

Figure 16: Calculated fractions of caesium (left) and molybdenum (right) released during the VERCORS 4 test with/without $Cs_2Mo_2O_7$ in the database compared to the mesurements. The second Y-scale refers to the temperature evolution during the tests

It appears that the formation of $Cs_2Mo_2O_{7(g)}$ is favored during the test compared to that of $Cs_2MoO_{4(g)}$. The proportion of Mo in the gas phase remains however small during the oxidation plateau (less than 10%) which explains the nearly null release during this part of the VERCORS 4 test. During the temperature ramp and the last plateau, 70% of the Mo in the fuel is now found in $Cs_2Mo_2O_{7(g)}$. As a consequence, the release of molybdenum is enhanced, reaching ∼65% at the end of the test. The Mo release is greatly improved compared to the calculation without $Cs_2Mo_2O_7$. Furthermore, the release of Cs is practically not modified as both $Cs_2MoO_{4(g)}$ and $Cs_2Mo_2O_{7(g)}$ include 2 moles of Cs per mole of compound.

5.2 Barium

The estimation of barium release during the VERCORS 4 test is close to the on-line measurements (Figure 14). The introduction of $Cs_2Mo_2O_7$ in the thermodynamic database does not change the results, which confirms that Ba speciation has little correlation with that of Mo. During the VERCORS 5 test, there is on the contrary an overestimation by a factor 2 of the barium released. The temperature at which barium starts to leave the fuel is however consistent with the measurements (Figure 14). Analysis of the barium speciation during the VERCORS 5 test shows that most of the barium in the fuel is found in $BaMoO_{4(g)}$ during the high temperature ramp and plateau (oxidizing conditions) which explains the too high released fraction. However, gamma tomography performed on the VERCORS 5 fuel cross section after the test showed that part of the barium released from the fuel pellets had reacted with the cladding [6][37][33]. Independent thermochemical calculations were made to analyze this issue. It was found that formation of $BaZrO_{3(s)}$ from Ba depended on both the applied oxido-reducing conditions and the quantity of Zr available in the system. In addition, Zr being partly soluble as $ZrO_{2(ss)}$ in the fuel, it is distributed between $BaZrO_{3(s)}$ and $ZrO_{2(ss)}$. In order to refine our thermodynamic database on this point, the species $ZrO_{2(ss)}$ was included in considering the thermodynamic functions available in the Thermodynamics Advanced Fuel-International Database (TAF-ID [32]).

5.2.1 VERCORS 5

To understand the actual Ba release in the VERCORS 5 test (with oxidizing conditions in the high temperature step), it is necessary to consider simultaneously the following major reactions in consistency with experimental observations:

$$BaMoO_{4(s)} = BaMoO_{4(g)} \tag{3}$$

$$BaZrO_{3(s)} = BaO_{(g)} + ZrO_{2(ss)} \tag{4}$$

$$BaZrO_{3(s)} + H_2O_{(g)} = BaH_2O_{2(g)} + ZrO_{2(ss)} \tag{5}$$

By considering the chemical reactions 3, 4 and 5, the following expression for the barium total partial pressure $p_{Ba(GAS)}$ in VERCORS 5 is obtained:

$$p_{Ba(GAS)} = K_3(T) + K_4(T) * \frac{1}{aZrO_{2(ss)}} + K_5(T) * \frac{p_{H_2O}}{aZrO_{2(ss)}} \tag{6}$$

where $K_i(T)(i=3, 4, 5)$ is the thermochemical equilibrium constant for the reaction (i), $aZrO_{2(ss)}$ is the $ZrO_{2(ss)}$ activity and p_{H_2O} is the water partial pressure in the gas phase. It appears from equation 6 that the barium partial pressure and thus the barium content in the gas phase (which drives the release) depends on both the Zr content (coming from the irradiated fuel

and the cladding) which forms $ZrO_{2(ss)}$ in the fuel and the steam content in the atmosphere. It is worthwhile to note that the $BaO_{(s)}$ phase, which is much less stable than $BaMoO_{4(s)}$ in oxidizing conditions, is unlikely to form in the Vercors-5 conditions, as shown in Figure 15. Consequently, in consistency with equation 6, the O_2 partial pressure (that is the ratio H_2O/H_2) should have a minor effect, if any, on the Ba release in steam atmosphere. The H_2O content only influences the Ba release. Observations from VERCORS 5 show furthermore that, in the same experimental conditions than Ba, ruthenium release is driven by the reaction Ru + H_2O = RuO_i + H_2, which only depends on the O_2 partial pressure ($\sim H_2O/H_2$). The release of Ru is thus a good indicator of the oxygen partial pressure p_{O_2} in the atmosphere, and thus an indicator of the residual H_2 in the steam carrier gas, after switching to the H_2O atmosphere during the high temperature step.

5.2.2 VERCORS 4

In the VERCORS 4 test (with reducing conditions in the high temperature step), it is necessary to include the following reaction, accounting for the reduction of molybdenum, in addition to the ones previously mentioned:

$$BaZrO_{3(s)} + Mo_{(s)} + 3H_2O = BaMoO_{4(g)} + ZrO_{2(ss)} + 3H_{2(g)} \tag{7}$$

In the Vercors-4 test, as well as in the Verdon-1 test [33], Mo is expected as metallic $Mo_{(s)}$ (pure compound) as soon as a reducing atmosphere is imposed at the end of the oxidation plateau, mostly resulting from the quantitative reduction of $MoO_{2(s)}$. According to the TAF-ID database in which a non-ideal model is available for Mo [33][32], the metallic $Mo_{(s)}$ phase undergoes a solid-liquid transition in the temperature range 2123°C-2160°C, during which Mo is involved into both the metallic $Mo_{(s)}$ phase and a liquid intermetallic phase (including Ru, Rh, Tc, Mo). From 2160°C onwards, when $Mo_{(s)}$ no longer exists, most Mo is found in the intermetallic alloy, as $Mo_{(ss)}$. Experimentally, the major part of Ba, if not all, is released in the temperature region in which the solid-liquid transition occurs, suggesting that metallic $Mo_{(s)}$ is still present inside the fuel. That is why we select the reaction 7 involving metallic $Mo_{(s)}$, of activity equal to unity, to assess the Ba release. Reaction 7 provides an additional term to the barium total partial pressure ($p_{Ba(GAS)}$) of equation 6 in the form:

$$p_{BaMoO_{4(g)}} = K_7(T) * \frac{1}{aZrO_{2(ss)}} * \left(\frac{p_{H_2O}}{p_{H_2}}\right)^3 \tag{8}$$

It should be noted that the formation of the $BaO_{(s)}$ phase is equally unlikely under the reducing conditions of the Vercors-4 test, the more stable $BaZrO_{3(s)}$ phase being favored. Nevertheless, as shown in equation 8, the O_2 partial pressure (that is the ratio H_2O/H_2) influences the stability of $Mo_{(sorss)}$, which can affect indirectly the Ba release in reducing atmosphere. It appears from equations 6 and 8 that in VERCORS 4, the total barium partial pressure (which drives the release) depends on:

- the Zr content (coming from both irradiated fuel and the cladding) which forms $ZrO_{2(ss)}$ in the fuel

- the H_2 content in the injected gas in the furnace
- the residual H_2O content in the injected gas in the furnace, after switching to the (He/H_2) atmosphere at the high temperature step.

An optimization of the Zr content in the system is thus needed to simulate accurately the Ba release in both VERCORS 4 and VERCORS 5 tests. In other words, the release of Ba at high temperature in a given atmosphere (steam or H_2) is an indicator of the extent of the cladding solubilization in the fuel. Furthermore, an estimation of the residual H_2O in the carrier gas is also needed to estimate at best the barium release in reducing conditions.

5.2.3 Optimized barium release

In order to validate the previous theoretical conclusions, simulations of the VERCORS 4 and VERCORS 5 tests were performed by adjusting the parameters of interest mentioned before, until best fittings of the Mo and Ba curves were obtained.

- In VERCORS 5, the H_2 residual content in the injected gas was estimated from the measured Ru release curve and the Zr content in the fuel was fitted from the measured Ba release curve. Best fittings were obtained with around 1% of residual H_2 in the H_2O carrier gas and 10% of the Zr cladding,
- In VERCORS 4, both the H_2O residual content and the Zr content were fitted from the measured Ba release curve. The optimal parameters were 1.2% of residual H_2O in the (He/H_2) carrier gas and around 2% of the Zr cladding.

Consistent values for the significant parameters (Zr content and residual H_2 or H_2O content) were obtained in both tests. The simulated release curves of Mo and Ba are in good agreement with the experimental ones, as shown in figure 17.

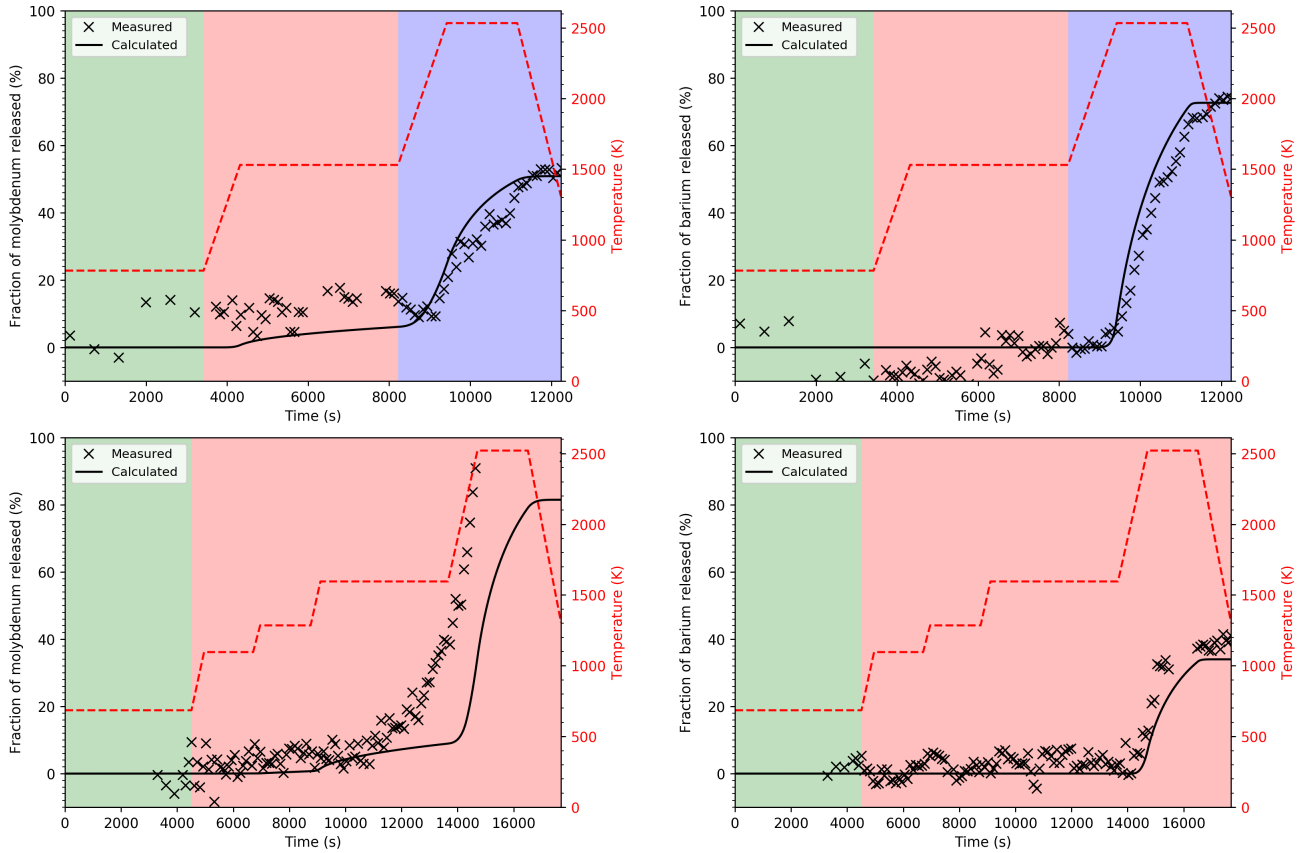

Figure 17: Calculated and measured fractions of molybdenum (left) and barium (right) released during the VERCORS 4 (top) and VERCORS 5 (bottom) tests with optimized parameters for the Zr content in the fuel, H_2O residual content (VERCORS 4) and H_2 residual content (VERCORS 5). The second Y-scale refers to the temperature evolution during the test.

With almost the same parameters for the Zr content and H_2O residual content (VERCORS 4) or H_2 residual content (VERCORS 5), a very good agreement between measures and calculations for both molybdenum and barium during a reducing test (VERCORS 4) and an oxidizing test (VERCORS 5) is obtained.

Conclusions

In this paper, the coupling of a gas diffusion model with thermochemical equilibrium calculations has been presented and applied to the VERCORS 4 and 5 tests, representative of severe accidents conditions. A simple gas diffusion model based on the equivalent sphere model was considered but improved to include the contribution of all the gases formed from the chemically-reactive Fission Products (source term in the diffusion equation). In this respect, FP release from the fuel is assumed to be driven by the same mechanism irrespective of the FPs considered. The main limitation to FP release is related to the chemical state of the FPs in the fuel, whether in the gas phase, the U-Pu-O-FPs solid solution phase or the condensed phases. The

estimation of the FP state relies on thermochemical equilibrium calculations performed at each time step.

The simulations results were compared to on-line measurements of FP release during the VERCORS 4 and 5 tests. Overall, the release kinetics of the volatile FPs (iodine, tellurium, caesium) were very well reproduced by the calculation, owing to the availability of these FPs in the gas phase. Part of the semi-volatile FP release kinetics (barium, molybdenum) were correctly assessed by the coupled approach showing the sensitivity to the external conditions (reducing in the VERCORS 4 test, oxidizing in the VERCORS 5 test).

It was shown that the simulation results on the semi-volatile FP molybdenum in reducing conditions could be greatly improved by the consideration of caesium dimolybdate in the database owing to its preferential formation in the gas phase. In oxidizing and reducing conditions, barium and molybdenum releases were found to depend mainly on the Zr coming from the fuel and the cladding (partly solubilized in the fuel) and on residual gases in the furnace. A good agreement with the barium and molybdenum releases kinetics was obtained by considering in the thermochemical calculations $\sim$2% of the cladding Zr in reducing conditions and $\sim$10% in oxidizing conditions together with $\sim$1% of residual gases (H_2 or H_2O) in the injected gas mixture. The consideration of part of the cladding is consistent with the trapping of barium in the cladding as observed after the VERCORS 5 test.

The straightforward coupling approach proposed in this paper is well suited for use in fuel performance codes or consideration with advanced thermodynamic databases able to deal with fuel-clad melting, such as the TAF-ID [32]. This is the topic of a companion paper [43].

Acknowledgements

The CEA authors would like to acknowledge EDF and FRAMATOME for their technical and financial support to this work. Special thanks are adressed to Jacques Léchelle from CEA for thermodynamic assesments and fruitful discussions.

References

[1] B.J. Lewis, R. Dickson, F.C. Iglesias, G. Ducros, and T. Kudo. Overview of experimental programs on core melt progression and fission product release behaviour. *Journal of Nuclear Materials*, 380(1-3):126–143, 2008.

[2] M. Schwarz, G. Hache, and P. von der Hardt. PHEBUS FP: a severe accident research programme for current and advanced light water reactors. *Nuclear Engineering and Design*, 187(1):47–69, 1999.

[3] JP. Leveque, B. Andre, G. Ducros, G. Lemarois, and G. Lhiaubet. The HEVA experimental program. *Nuclear Technology*, 108(1):33–44, 1994.

[4] Y. Pontillon, G. Ducros, and P.P. Malgouyres. Behaviour of fission products under severe PWR accident conditions vercors experimental program — Part 1: General description of the programme. *Nuclear Engineering and Design*, 240(7):1843 – 1852, 2010.

[5] Y. Pontillon, G. Ducros, and P.P. Malgouyres. Behaviour of fission products under severe PWR accident conditions: The vercors experimental program — Part 2: Release and transport of fission gases and volatile fission products. *Nuclear Engineering and Design*, 240(7):1853 – 1866, 2010.

[6] Y. Pontillon, G. Ducros, and P.P. Malgouyres. Behaviour of fission products under severe PWR accident conditions. the vercors experimental program — Part 3: Release of low-volatile fission products and actinides. *Nuclear Engineering and Design*, 240(7):1867 – 1881, 2010.

[7] G Ducros, P.P Malgouyres, M Kissane, D Boulaud, and M Durin. Fission product release under severe accidental conditions: general presentation of the program and synthesis of VERCORS 1–6 results. *Nuclear Engineering and Design*, 208(2):191 – 203, 2001.

[8] Y. Pontillon, E. Geiger, C. Le Gall, S. Bernard, A. Gallais-During, P.P. Malgouyres, E. Hanus, and G. Ducros. Fission products and nuclear fuel behaviour under severe accident conditions. Part 1: main lessons learnt from the first VERDON test. *Journal of Nuclear Materials*, 495:363 – 384, 2017.

[9] E. Geiger, C. Le Gall, A. Gallais-During, Y. Pontillon, J. Lamontagne, E. Hanus, and G. Ducros. Fission products and nuclear fuel behaviour under severe accident conditions. Part 2: Fuel behaviour in the VERDON-1 sample. *Journal of Nuclear Materials*, 495:49 – 57, 2017.

[10] C. Le Gall, E. Geiger, A. Gallais-During, Y. Pontillon, J. Lamontagne, E. Hanus, and G. Ducros. Fission products and nuclear fuel behaviour under severe accident conditions. Part 3: speciation of fission products in the VERDON-1 sample. *Journal of Nuclear Materials*, 495:291 – 298, 2017.

[11] G. Brillant, C. Marchetto, and W. Plumecocq. Fission product release from nuclear fuel. I. physical modelling in the ASTEC code. *Annals of Nuclear Energy*, 61:88 – 95, 2013.

[12] G. Brillant, C. Marchetto, and W. Plumecocq. Fission product release from nuclear fuel. II. validation of ASTEC/ELSA on analytical and large scale experiments. *Annals of Nuclear Energy*, 61:96–101, 2013.

[13] D.R. Olander and V. Mubayi. Review of the materials-chemistry models in the VICTORIA code. *Journal of Nuclear Materials*, 270(1-2):1–10, 1999.

[14] R. Gauntt. MELCOR 1.8.5 modeling aspect of fission product release, transport and deposition. Technical report, Sandia National laboratory, 2010.

[15] M.S. Veshchunov, V.D. Ozrin, V.E. Shestak, V.I. Tarasov, R. Dubourg, and G. Nicaise. Development of the mechanistic code MFPR for modelling fission-product release from irradiated UO_2 fuel. *Nuclear Engineering and Design*, 236(2):179 – 200, 2006.

[16] M.S. Veshchunov, R. Dubourg, V.D. Ozrin, V.E. Shestak, and V.I. Tarasov. Mechanistic modelling of urania fuel evolution and fission product migration during irradiation and heating. *Journal of Nuclear Materials*, 362(2):327 – 335, 2007.

[17] J. Sercombe, B. Michel, and C. Riglet-Martial. 2.14 - modelling of pellet cladding interaction. In R.J.M. Konings and R.E. Stoller, editors, *Comprehensive Nuclear Materials*. Elsevier, Oxford, 2020.

[18] B. Baurens, J. Sercombe, C. Riglet-Martial, L. Desgranges, L. Trotignon, and P. Maugis. 3D thermo-chemical–mechanical simulation of power ramps with ALCYONE fuel code. *Journal of Nuclear Materials*, 452(1):578–594, 2014.

[19] P. Konarski, J. Sercombe, C. Riglet-Martial, L. Noirot, I. Zacharie-Aubrun, K. Hanifi, M. Frégonèse, and P. Chantrenne. 3D simulation of a power ramp including fuel thermochemistry and oxygen thermodiffusion. *Journal of Nuclear Materials*, 519:104–120, 2019.

[20] L. Noirot. MARGARET: A comprehensive code for the description of fission gas behavior. *Nuclear Engineering and Design*, 241(6):2099 – 2118, 2011.

[21] C. Introïni, J. Sercombe, and B. Sundman. Development of a robust, accurate and efficient coupling between PLEIADES/ALCYONE 2.1 fuel performance code and the OpenCalphad thermo-chemical solver. *Nuclear Engineering and Design*, 369, 2020.

[22] J.-C. Dumas. *Study of the JOG formation in sodium fast reactors: modeling of volatile fission products*. PhD thesis, Institut National Polytechnique, Grenoble, France, 1995.

[23] H. Loukusa, T. Ikonen, V. Valtavirta, and V. Tulkki. Thermochemical modeling of nuclear fuel and the effects of oxygen potential buffers. *Journal of Nuclear Materials*, 481:101–110, 2016.

[24] B. Sundman, U.R. Kattner, M. Palumbo, and S.G. Fries. Opencalphad-a free thermodynamic software. *Integrating Materials and Manufacturing Innovation*, 4(1):1, 2015.

[25] B. Sundman, L. Xiao-Gang, and O. Hiroshi. The implementation of an algorithm to calculate thermodynamic equilibria for multi-component systems with non-ideal phases in a free software. *Computational Materials Science*, 101:127–137, 2015.

[26] C.W. Bale, E. Bélisle, P. Chartrand, S.A. Decterov, G. Eriksson, A.E. Gheribi, K. Hack, I.-H. Jung, Y.-B. Kang, J. Melançon, A.D. Pelton, S. Petersen, C. Robelin, J. Sangster, P. Spencer, and M-A. Van Ende. Factsage thermochemical software and databases, 2010–2016. *Calphad*, 54:35 – 53, 2016.

[27] A. Germain, J. Sercombe, C. Riglet-Martial, Y. Pontillon, L. Noirot, C. Introini, and P. Maugis. Modeling of fission gas release and irradiated fuel thermochemistry during severe accidents. *Topfuel conference*, September 2019.

[28] T.B. Lindemer and T.M. Besmann. Chemical thermodynamic representation of UO_2. *Journal of Nuclear Materials*, 130:473–488, 1985.

[29] T.B. Lindemer and J. Brynestad. Review and chemical thermodynamic representation of U_{1-z} $Ce_zO_{2\pm x}$ and $U_{1-z}Ln_zO_{2\pm x}$; Ln= Y, La, Nd, Gd. *Journal of the American Ceramic Society*, 69(12):867–876, 1986.

[30] P. Konarski. *Thermo-chemical-mechanical modeling of nuclear fuel behavior. Impact of oxygen transport in the fuel on Pellet Cladding Interaction.* PhD thesis, INSA de Lyon, France, October 2019.

[31] Ch. Riglet-Martial, J. Sercombe, and Y. Pontillon. Speciation and release kinetics of the fission products Mo, Cs, Ba and I from nuclear fuels in severe accident conditions. *Topfuel conference*, 2018.

[32] C. Guéneau, N. Dupin, L. Kjellqvist, E. Geiger, M. Kurata, S. Gossé, E. Corcoran, A. Quaini, R. Hania, A.L. Smith, et al. TAF-ID: An international thermodynamic database for nuclear fuels applications. *Calphad*, 72, 2021.

[33] E. Geiger, C. Guéneau, Y. Pontillon, and E.C. Corcoran. Modelling nuclear fuel behaviour with TAF-ID: Calculations on the VERDON-1 experiment, representative of a nuclear severe accident. *Journal of Nuclear Materials*, 522:294–310, 2019.

[34] A.H. Booth. A method of calculating fission gas diffusion from UO_2 fuel and its application to the X-2-f loop test. Technical report, Atomic Energy of Canada Limited, 1957.

[35] D.R. Olander. Mechanistic interpretations of UO_2 oxidation. *Journal of Nuclear Materials*, 252(1):121 – 130, 1998.

[36] L. Desgranges, T. Blay, J. Lamontagne, I. Roure, and P. Bienvenu. Fission products behaviour during a power transient: Their inventory in an intragranular bubble. *Journal of Nuclear Materials*, 493:225–229, 2017.

[37] G. Brillant, C. Marchetto, and W. Plumecocq. Ruthenium release from fuel in accident conditions. *Radiochimica Acta*, 98, 2010.

[38] C. Le Gall. *Contribution to the study of fission products release from nuclear fuels in severe accident conditions: effect of the pO2 on Cs, Mo and Ba speciation.* PhD thesis, Grenoble Alpes University, France, November 2018.

[39] C. Riglet-Martial, J. Sercombe, J. Lamontagne, J. Noirot, I. Roure, T. Blay, and L. Desgranges. Experimental evidence of oxygen thermo-migration in PWR UO_2 fuels during power ramps using in-situ oxido-reduction indicators. *Journal of Nuclear Materials*, 480:32–39, 2016.

[40] T.M.D Do, S. Sujatanond, Y. Tachibana, and T. Ogawa. Vaporization and deposition of cesium dimolybdate, $Cs_2Mo_2O_7$. *Journal of Nuclear Science and Technology*, 54(3):330–336, 2017.

[41] A.L. Smith, G. Kauric, L. van Eijck, K. Goubitz, G. Wallez, J.-C. Griveau, E. Colineau, Nicolas Clavier, and R.J.M. Konings. Structural and thermodynamic study of dicesium molybdate $Cs_2Mo_2O_7$: Implications for fast neutron reactors. *Journal of Solid State Chemistry*, 253:89–102, September 2017.

[42] A.L. Smith, J. Vlieland, M.-C. Pignié, M. Abbink, G. Mikaelian, and P. Benigni. New insights into the Cs-Mo-O system: Experimental studies of the Cs_2MoO_4-MoO_3 pseudo-binary system. *Thermochimica Acta*, 696, February 2021.

[43] A. Germain, J. Sercombe, C. Riglet-Martial, C. Introini, L. Noirot, Y. Pontillon, P. Maugis, and C. Guéneau. Modeling of high burnup fuel thermochemistry, fission products release and fuel melting during the VERDON 1 and RT6 tests. *Submitted to the Journal of Nuclear Materials*, 2021.

A Compounds considered in the TBASE for the thermochemical equilibrium calculations

The following phases and compounds are considered in the updated TBASE:

- The gas phase includes the following compounds: $Ba_{(g)}$, $Ba_{2(g)}$, $BaH_{(g)}$, $BaH_2O_{2(g)}$, $BaI_{(g)}$, $BaI_{2(g)}$, $BaMoO_{4(g)}$, $BaO_{(g)}$, $BaHO_{(g)}$, $Ba_2O_{(g)}$, $Ba_2O_{2(g)}$, $Ce_{(g)}$, $CeO_{(g)}$, $Cr_{(g)}$, $CrO_{(g)}$, $CrO_{2(g)}$, $CrO_{3(g)}$, $Cs_{(g)}$, $Cs_{2(g)}$, $CsI_{(g)}$, $Cs_2I_{2(g)}$, $Cs_2MoO_{4(g)}$, $Cs_2O_{(g)}$, $Cs_2O_{2(g)}$, $CsO_{(g)}$, $CsHO_{(g)}$, $Eu_{(g)}$, $EuO_{(g)}$, $Eu_2O_{2(g)}$, $GdO_{(g)}$, $H_{(g)}$, $He_{(g)}$, $H_{2(g)}$, $HO_{(g)}$, $HO_{2(g)}$, $H_2O_{2(g)}$, $H_2O_{(g)}$, $HTe_{(g)}$, $HMo_{3(g)}$, $HMoO_{(g)}$, $HMoO_{2(g)}$, $H_2MoO_{2(g)}$, $H_2MoO_{3(g)}$, $H_2MoO_{4(g)}$, $I_{(g)}$, $I_{2(g)}$, $LaO_{(g)}$, $Mo_{(g)}$, $Mo_{2(g)}$, $MoI_{(g)}$, $MoI_{2(g)}$, $MoI_{3(g)}$, $MoI_{4(g)}$, $MoO_{(g)}$, $MoO_{2(g)}$, $MoO_{3(g)}$, $Mo_2O_{6(g)}$, $Mo_3O_{9(g)}$, $Mo_4O_{12(g)}$, $Mo_5O_{15(g)}$, $MoO_2I_{2(g)}$, $O_{(g)}$, $O_{2(g)}$, $O_{3(g)}$, $Pd_{(g)}$, $PdO_{(g)}$, $Pu_{(g)}$, $PuO_{(g)}$, $PuO_{2(g)}$, $Ru_{(g)}$, $RuO_{(g)}$, $RuO_{2(g)}$, $RuO_{3(g)}$, $RuO_{4(g)}$, $Te_{(g)}$, $Te_{2(g)}$, $Te_{3(g)}$, $Te_{4(g)}$, $Te_{5(g)}$, $Te_{6(g)}$, $Te_{7(g)}$, $TeI_{2(g)}$, $TeO_{(g)}$, $TeO_{2(g)}$, $Te_2O_{2(g)}$, $TeOI_{2(g)}$, $U_{(g)}$, $UO_{(g)}$, $UO_{2(g)}$, $UO_{3(g)}$, $U_2O_{2(g)}$, $U_2O_{3(g)}$, $U_2O_{4(g)}$, $U_2O_{5(g)}$, $U_2O_{6(g)}$, $Zr_{(g)}$, $ZrI_{(g)}$, $ZrI_{2(g)}$, $ZrI_{3(g)}$, $ZrI_{4(g)}$, $ZrO_{(g)}$, $ZrO_{2(g)}$.

- The liquid stoichiometric compounds included are: $Ba_{(l)}$, $BaH_2O_{2(l)}$, $BaI_{2(l)}$, $BaO_{(l)}$, $Ce_{(l)}$, $CeO_{2(l)}$, $Ce_2O_{3(l)}$, $Cr_{(l)}$, $CrO_{(l)}$, $Cs_{(l)}$, $CsHO_{(l)}$, $CsI_{(l)}$, $Cs_2MoO_{4(l)}$, $Cs_2O_{(l)}$, $Cs_2O_{2(l)}$, $CsO_{2(l)}$, $Eu_{(l)}$, $EuO_{(l)}$, $Eu_2O_{3(l)}$, $Gd_{(l)}$, $Gd_2O_{3(l)}$, $H_2O_{(l)}$, $H_2O_{2(l)}$, $I_{2(l)}$, $La_{(l)}$, $Mo_{(l)}$, $MoO_{3(l)}$, $Pd_{(l)}$, $Pu_{(l)}$, $PuO_{2(l)}$, $Pu_2O_{3(l)}$, $Ru_{(l)}$, $RuO_{4(l)}$, $Te_{(l)}$, $TeO_{2(l)}$, $U_{(l)}$, $UO_{2(l)}$, $Zr_{(l)}$, $ZrI_{2(l)}$, $ZrI_{3(l)}$, $ZrI_{4(l)}$, $ZrO_{2(l)}$.

- The solid stoichiometric compounds included are: $Ba_{(s)}$, $BaH_2O_{2(s)}$, $BaI_{2(s)}$, $BaMoO_{4(s)}$, $BaO_{(s)}$, $BaTe_{(s)}$, $BaUO_{4(s)}$, $BaZrO_{3(s)}$, $Ce_{(s)}$, $Ce_2O_{3(s)}$, $Cr_{(s)}$, $Cr_2O_{3(s)}$, $Cs_{(s)}$, $CsHO_{(s)}$, $CsI_{(s)}$, $Cs_2MoO_{4(s)}$, $Cs_2O_{(s)}$, $Cs_2O_{2(s)}$, $CsO_{2(s)}$, $Cs_2Te_{(s)}$, $Cs_2TeO_{3(s)}$, $Cs_2Te_4O_{9(s)}$, $Cs_2Te_4O_{12(s)}$, $Cs_2TeO_{4(s)}$, $Cs_2UO_{4(s)}$, $Cs_2U_4O_{12(s)}$, $Eu_{(s)}$, $Eu_2O_{3(s)}$, $Gd_{(s)}$, $Gd_2O_{3(s)}$, $I_{2(s)}$, $La_{(s)}$, $La_2O_{3(s)}$, $LaZr_2O_{7(s)}$, $MoI_{2(s)}$, $MoI_{3(s)}$, $MoI_{4(s)}$, $MoO_{2(s)}$, $MoO_{3(s)}$, $PdO_{(s)}$, $Pu_{(s)}$, $PuO_{(s)}$, $Pu_2O_{3(s)}$, $RuO_{2(s)}$, $RuTe_{2(s)}$, $Te_{(s)}$, $TeO_{2(s)}$, $U_{(s)}$, $UO_{3(s)}$, $U_3O_{8(s)}$, $U_4O_{9(s)}$, $U_3PuO_{8(s)}$, $Zr_{(s)}$, $ZrI_{2(s)}$, $ZrI_{3(s)}$, $ZrI_{4(s)}$, $ZrTe_{2(s)}$.

- The metal phase includes the following compounds: $Mo_{(s)}$, $Ru_{(s)}$, $Pd_{(s)}$.

- The solid solution phase includes the following compounds: $Ce_{3/4(ss)}$, $CeO_{2(ss)}$, $CrO_{3/2(ss)}$, $EuO_{(ss)}$, $Eu_{4/3}O_{2(ss)}$, $Gd_{4/3}O_{2(ss)}$, $La_{4/3}O_{2(ss)}$, $PuO_{2(ss)}$, $Pu_{4/3}O_{2(ss)}$, $U_{1/3(ss)}$, $UO_{2(ss)}$, $U_3O_{7(ss)}$, $UEuO_{3.83(ss)}$, $UGd_2O_{6(ss)}$, $ULa_2O_{6(ss)}$, $U_{1/3}Pu_{4/3}O_{2(ss)}$, $ZrO_{2(ss)}$.